

See discussions, stats, and author profiles for this publication at: <https://www.researchgate.net/publication/272028212>

Overview of the Liulin type instruments for space radiation measurement and their scientific results

Article in Life sciences and space research · February 2015

DOI: 10.1016/j.lssr.2015.01.005

CITATIONS

6

READS

343

22 authors, including:



Tsvetan Dachev

Bulgarian Academy of Sciences

173 PUBLICATIONS 1,189 CITATIONS

[SEE PROFILE](#)



Jordanka Semkova

Bulgarian Academy of Sciences

53 PUBLICATIONS 306 CITATIONS

[SEE PROFILE](#)



Vyacheslav Shurshakov

Институт медико-биологических пр...

163 PUBLICATIONS 979 CITATIONS

[SEE PROFILE](#)



V.V. Benghin

Институт медико-биологических пр...

67 PUBLICATIONS 401 CITATIONS

[SEE PROFILE](#)

Some of the authors of this publication are also working on these related projects:



Daphniatox - a new bioassay to determine toxicity in aquatic ecosystems [View project](#)



DEPRON [View project](#)

All content following this page was uploaded by [Vyacheslav Shurshakov](#) on 22 February 2015.

The user has requested enhancement of the downloaded file. All in-text references [underlined in blue](#) are added to the original document and are linked to publications on ResearchGate, letting you access and read them immediately.



Overview of the Liulin type instruments for space radiation measurement and their scientific results



T.P. Dachev ^{a,*}, J.V. Semkova ^a, B.T. Tomov ^a, Yu.N. Matviichuk ^a, P.G. Dimitrov ^a, R.T. Koleva ^a, St. Malchev ^a, N.G. Bankov ^a, V.A. Shurshakov ^b, V.V. Benghin ^b, E.N. Yarmanova ^b, O.A. Ivanova ^b, D.-P. Häder ^c, M. Lebert ^d, M.T. Schuster ^d, G. Reitz ^e, G. Horneck ^e, Y. Uchihori ^f, H. Kitamura ^f, O. Ploc ^g, J. Cubancak ^g, I. Nikolaev ^h

^a Space Research and Technology Institute, Bulgarian Academy of Sciences, Sofia, Bulgaria

^b State Research Center Institute of Biomedical Problems, Russian Academy of Science, Moscow, Russia

^c Neue Str. 9, 91096 Möhrendorf, Germany

^d Friedrich-Alexander-Universität, Department for Biology, Erlangen, Germany

^e DLR, Institute of Aerospace Medicine, Köln, Germany

^f National Institute of Radiological Sciences-STA, Chiba, Japan

^g Nuclear Physics Institute, Czech AS, Prague, Czech Republic

^h S.P. Korolev Rocket and Space Corporation Energia, Moscow, Russia

ARTICLE INFO

Article history:

Received 6 December 2014

Received in revised form 15 January 2015

Accepted 26 January 2015

Keywords:

Space radiation

Dosimetry

ISS

GCR

SAA

ABSTRACT

Ionizing radiation is recognized to be one of the main health concerns for humans in the space radiation environment. Estimation of space radiation effects on health requires the accurate knowledge of the accumulated absorbed dose, which depends on the global space radiation distribution, solar cycle and local shielding generated by the 3D mass distribution of the space vehicle. This paper presents an overview of the spectrometer-dosimeters of the Liulin type, which were developed in the late 1980s and have been in use since then. Two major measurement systems have been developed by our team. The first one is based on one silicon detector and is known as a Liulin-type deposited energy spectrometer (DES) (Dachev et al., 2002, 2003), while the second one is a dosimetric telescope (DT) with two or three silicon detectors. The Liulin-type instruments were calibrated using a number of radioactive sources and particle accelerators. The main results of the calibrations are presented in the paper. In the last section of the paper some of the most significant scientific results obtained in space and on aircraft, balloon and rocket flights since 1989 are presented.

© 2015 The Committee on Space Research (COSPAR). Published by Elsevier Ltd. All rights reserved.

1. Introduction

Much of the Earth's surface where people live and work has a natural soil cover resulting from weathering processes. The lower atmospheric radiation and the associated external exposure result mainly from gamma rays emitted from the top 25 cm of the surface layer of the Earth and from building construction materials (Wilson et al., 2003). At ground level space radiation (originating from outside the Earth's atmosphere, including solar radiation) produces about 11% of the effective dose to the average US population, while terrestrial radiation (emitted by radionuclides in soil

and rocks) accounts for an additional 7%. Most of the effective dose affecting the general population is produced by inhaled radon and ingested potassium, thorium and uranium (Wahl, 2010).

There are three principal sources of primary ionizing radiation in low Earth orbit (LEO): (1) galactic cosmic rays (GCR); (2) energetic electrons and protons trapped in the geomagnetic field that make up the Earth's radiation belts and (3) solar energetic particles (SEP), high fluxes of charged particles emitted during sporadic but intense solar flares and coronal mass ejections (CME). In low Earth orbit (LEO), a fourth source, albedo neutrons and protons, is also encountered (Benton and Benton, 2001). Dose characteristics in the near Earth space radiation environment depend on factors such as orbit parameters, solar cycle phase and current helio- and geophysical conditions.

* Corresponding author. Tel.: +359887366225.

E-mail address: tdachev@bas.bg (T.P. Dachev).

1.1. Galactic cosmic rays

The dominant radiation component in the near Earth and free space environment are the galactic cosmic rays. The GCR are charged particles that originate from sources beyond the solar system. GCR are the most penetrating of the major types of ionizing radiation. The energies of GCR particles range from several eV up to 10^{12} MeV/nucleon (MeV/n). The GCR spectrum consists of 98% protons and heavier ions (baryon component) and 2% electrons and positrons (lepton component). The baryon component is composed of 87% protons, 12% helium ions (alpha particles) and 1% heavy ions (Simpson, 1983). Highly energetic particles in the heavy ion component, typically referred to as high Z (Z is the atomic number) and energy (HZE) particles, play a particularly important role in space dosimetry (Horneck, 1994; Benton and Benton, 2001). HZE particles, especially iron, are characterized by high-LET (linear energy transfer) and are highly penetrating, giving them a large potential for radiobiological damage (Kim et al., 2010). Up to 1 GeV/n energy, the flux and spectra of GCR particles show modulation that is anti-correlated with solar activity. The daily GCR absorbed dose rates measured with the R3DE instrument (Dachev et al., 2012a) outside of the ISS at about 360 km altitude vary in the range $77\text{--}102 \mu\text{Gy d}^{-1}$ with an average of $91 \mu\text{Gy d}^{-1}$. GCR dose rates are higher when the surrounding material density is higher. These higher dose rate values are produced by additional secondary particles generated in the heavier shielding.

The natural radiation level at aircraft cruising altitudes at middle latitudes is about 20–30 times higher than at ground level. The radiation field arises as a result of the interaction of primary GCR particles with the Earth's atmosphere. An additional flux of albedo secondary GCR is observed at altitudes below 3 km, which contributes to the forming of the flux and dose rate minimum around 1.6 km altitude (Bazilevskaya et al., 2013). The intensity of the atmospheric radiation composed of GCR primary and secondary particles and their energy distribution vary with altitude, location in the geomagnetic field and the point in the Sun's magnetic activity (solar) cycle (Mertens et al., 2010, 2012, 2013).

The atmosphere provides shielding, which depends on the overhead atmospheric depth. The geomagnetic field provides a different kind of shielding, by deflecting low-momentum charged particles back to space. Because of the orientation of the geomagnetic field, which is predominantly dipolar in nature, the polar regions are susceptible to penetrating GCR and SEP particles. At each geographic location, a vertically incident particle has a minimum momentum per unit charge (magnetic rigidity) and can reach a given location above the Earth. This is known as the geomagnetic vertical cutoff rigidity (Shea and Smart, 2001). The local flux of incident GCR at a given time varies widely with geomagnetic location and the solar modulation level. When solar activity is high the GCR flux is low and vice versa.

1.2. Trapped radiation belts

Radiation belts are the regions of high concentration of energetic electrons and protons trapped within the Earth's magnetosphere. There are two distinct belts of toroidal shape surrounding the Earth where high energy charged particles are trapped in the geomagnetic field. The inner radiation belt (IRB), located between about 1.1 and 2 Earth radii, consists of electrons with energies up to 10 MeV and protons with energies up to ~ 700 MeV. The outer radiation belt (ORB) starts from about 4 Earth radii and extends to about 9–10 Earth radii in the anti-sun direction. The outer belt consists mostly of electrons whose energy is below 10 MeV. The electron flux may cause problems for components located outside a spacecraft (e.g. solar cell degradation). They do not have enough

energy to penetrate a heavily shielded spacecraft such as the International Space Station (ISS) wall, but may deliver large additional doses to astronauts during extravehicular activity (EVA) (Dachev et al., 2009, 2012b and 2013b). The South-Atlantic Anomaly (SAA) is an area where the IRB comes closer to the Earth's surface due to a displacement of the magnetic dipole axes from the Earth's center. The daily average SAA doses reported by Reitz et al. (2005) inside of the ISS vary in the range $74\text{--}215 \mu\text{Gy d}^{-1}$ for the absorbed dose rates and in the range $130\text{--}258 \mu\text{Sv d}^{-1}$ for the averaged equivalent daily dose rates.

The reduction of atmospheric density due to the diminishing solar activity leads to a long-term enhancement of the dose rate and particle flux in the SAA (Dachev et al., 1999a).

1.3. Solar Energetic Particles (SEP)

The SEP are mainly produced by solar flares, caused by sporadic eruptions of the chromosphere of the Sun. High fluxes of charged particles (mostly protons, electrons and helium and heavier ions) with energies up to several GeV are emitted by processes of acceleration outside the Sun. It is now generally understood that SEP events arise from coronal mass ejections (CME) from active regions of the solar surface. The CME propagates through interplanetary space carrying along with it the local surface magnetic field frozen into the ejected mass. There is a transition (shock) region between the normal sectored magnetic structure of interplanetary space and the fields frozen into the ejected mass, in which the interplanetary gas is accelerated, forming the SEP. As the accelerated region passes an observation point, the flux intensity is observed to increase dramatically (Mertens et al., 2010, 2012, 2013).

The time profile of a typical SEP starts with a rapid exponential increase in flux, reaching a peak in minutes to hours. The ion energies lie between 15 and 500 MeV/nucleon $^{-1}$ and the intensity can reach $10^4 \text{ cm}^{-2} \text{ s}^{-1} \text{ sr}^{-1}$. Electrons with energies of ~ 0.5 to 1 MeV arrive at the Earth, usually traveling along interplanetary field lines, within tens of minutes to tens of hours. Protons with energies of 20 to 80 MeV arrive within a few to ~ 10 h, although some high energy protons can arrive in as little as 20 minutes. SEPs are relatively rare and occur most often during the solar maximum phase of the approximately 11-year solar cycle. In years of maximum solar activity up to ten flares can occur, during the years of minimum solar activity only one event may be observed on average (Lantos, 1993).

2. Instrumentation

Instruments and methods used for space radiation dosimetry were recently reviewed by Caffrey and Hamby (2010). In the abstract of their paper they wrote: "The passive detection methods include track-etch, luminescent, nuclear emulsion, and metal foil detectors. These can provide a reliable source of data for all types of radiation, but often require processing that cannot occur in space. Experimental methods of LET determination using TLDs, such as the high temperature peak ratio (HTR) method, are also discussed. Portable readout passive detectors including Pille, MOSFET, and bubble detector systems provide a novel alternative to traditional passive detectors, but research is more limited and their widespread use has yet to be established. Active detectors including DOSTEL, CPDS, RRMID-III, TEPC, R-16, BBNID, and the Liulin series are examined for technical details. These instruments allow the determination of dose in real-time, and some can determine LET of incident particles by measuring energy deposition over a known path-length, but size and power consumption limit their practical use for dosimetry."

The first Liulin device (see Table 1, Part 1, Item No. 1) was developed for the scientific program of the second Bulgarian cos-

Table 1
Liulin type experiments performed during satellite missions.

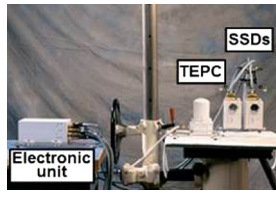
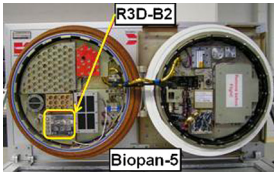
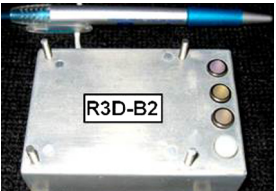
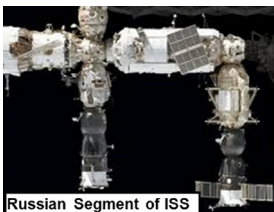
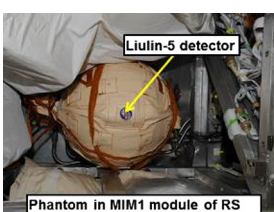
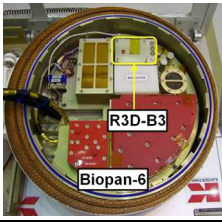
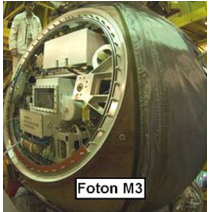
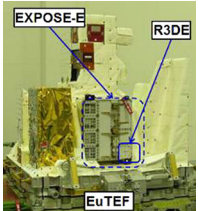
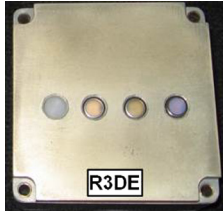
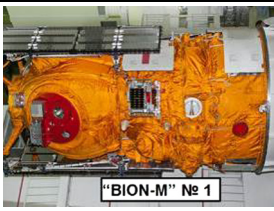
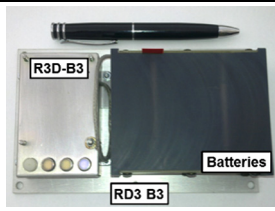
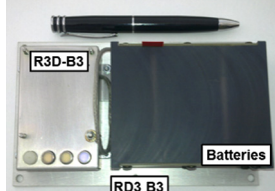
Part 1					
Item No.	Satellite	Experiment name	Instrument	Instrument location image	External view of the instrument
	Date begin–Date end	PI CoPI	Size [mm]/Mass [kg] Place Shielding [g cm^{-2}] Resolution [s]/[min]		
	Available number of measurements	References Cooperation			
1	MIR SS 04/1988–06/1994	LIULIN V. Petrov, IMBP; Ts. Dachev, SRTI. >2,000,000 measurements (Dachev et al., 1989) Bulgaria, Russia	LIULIN 1 DU (109 × 149 × 40 mm, 0.45 kg); 1 MCU (300 × 220 × 187 mm, 6.5 kg) Inside different modules of the MIR SS >5 g cm^{-2} 30 s	 MIR SS	 LIULIN-DU  LIULIN-MCU
2	Mars-96 16/11/1996 (The satellite was lost because of rocket booster malfunctioning)	RADIUS-MD V. Petrov, IMBP; Ts. Dachev, SRTI. (Semkova et al., 1994) Bulgaria, Russia, France	2 Solid State Detectors (SSD) (154 × 80 × 70 mm, 0.38 kg) Outside and inside Of the Mars-96 satellite >2 g cm^{-2} ; 10 min	 Mars-96 orbiter	 SSDs TEPC Electronic unit
3	ISS 05/05/2001– 26/08/2001/ 1,267,200 (Reitz et al., 2005); (Dachev et al., 2002) Bulgaria, Germany	ESA, Dosimetric Mapping G. Reitz, DLR; Ts. Dachev, SRTI. Liulin-E094	1 CIU (120 × 80 × 60 mm, 0.4 kg) 4 MDU (100 × 64 × 24 mm, 0.23 kg) Inside of the American Lab. and Node 1 of the ISS >20 g cm^{-2} ; 30 s	 Liulin MDU ISS002E7720 2001/06/29 15:35	 Electronic unit
4	Foton M2 01/06/2005– 12/06/2005 17,280 (Häder et al., 2009) Bulgaria, Germany	ESA, Biopan 5 G. Horneck, DLR; D. Häder, UER; Ts. Dachev, SRTI. R3D-B2	(57 × 82 × 24 mm, 0.12 kg) DU outside of the satellite and inside of the Biopan-5 facility 1.75 g cm^{-2} ; 60 s	 R3D-B2 Biopan-5	
5	ISS Since Sept. 2005 13/08/2008– 29/08/2008 Service system in next 15 years 149,760 spectra (Dachev et al., 1999b) Bulgaria, Russia, Belgium	Liulin-ISS V. Petrov, IMBP; Ts. Dachev, SRTI. Liulin-MKS	1 CIU (120 × 80 × 20 mm, 0.4 kg) 4 MDU (110 × 80 × 25 mm, 0.23 kg) Inside the Russian segment of ISS >20 g cm^{-2} ; 10–3599 s	 Russian Segment of ISS	 Liulin-ISS MDU
6	ISS 17/05/2007 Working permanently = Data recorded on memory card >2,500,000 measurements (Semkova et al., 2003, 2008) Bulgaria, Russia,	Matroska-R V. Petrov, IMBP; J. Semkova, SRTI. Liulin-5, Dosimetric telescope by 3 detectors ($\Phi 50/30 \times 191$ mm, 0.4 kg) Electronic block (160 × 90 × 30 mm, 0.8 kg)	Inside the Russian segment of the ISS; >20 g cm^{-2} ; 20 or 90 s for dose rate and flux, 15 or 85 min for LET and deposited energy spectra	 Liulin-5 detector Phantom in MIM1 module of RS	 Liulin-5 Electronic Liulin-5 Detector

Table 1 (continued)

Part 1					
Item No.	Satellite	Experiment name	Instrument	Instrument location image	External view of the instrument
	Date begin–Date end	PI CoPI	Size [mm]/Mass [kg] Place Shielding [g cm^{-2}] Resolution [s]/[min]		
	Available number of measurements	References Cooperation			
7	Foton M3 14/09/2007– 26/09/2007 18,720	ESA, Biopan 6 G. Horneck, DLR; D. Häder, UE; Ts. Dachev, SRTI. (Häder et al., 2009); (Damasso et al., 2009) Bulgaria, Germany	R3D-B3 1 DU ($57 \times 82 \times 24$ mm, 0.12 kg) Outside of the satellite and inside of the Biopan-6 facility 0.8 g cm^{-2} ; 60 s	 	
Part 2					
8	Foton M3 14/09/2007– 26/09/2007 27,360	ESA, PHOTO-II M.-T. Giardy, IC-AR, Rome, Italy; Ts. Dachev, SRTI. (Damasso et al., 2009) Bulgaria, Italy	Liulin-Photo, 1 DU ($57 \times 82 \times 24$ mm, 0.5 kg) Above Photo instrument, inside of the satellite, $>5.0 \text{ g cm}^{-2}$; 60 s	 	
9	ISS, Columbus module 17/02/2008– 03/09/2009 4,406,400	ESA, EXPOSE-E G. Horneck, DLR; D. Häder, UE; Ts. Dachev, SRTI. (Horneck et al., 1998), (Dachev et al., 2012a) Bulgaria, Germany	R3DE 1 DU ($76 \times 76 \times 36$ mm, 0.19 kg) Outside of ISS in the EXPOSE-E facility in EuTEF $>0.6 \text{ g cm}^{-2}$; 10 s	 	
10	Chandrayaan-1 satellite around the Moon 22/10/2008– 29/09/2009 1,209,600 spectra	RADOM Ts. Dachev, SRTI (Dachev et al., 2011c) Bulgaria, India	RADOM 1 DU ($110 \times 40 \times 20$ mm, 0.098 kg) Outside of the Chandrayaan-1 satellite $>0.6 \text{ g cm}^{-2}$; 10 and 30 s	 	
11	ISS, Zvezda module 11/03/2009– 20/08/2010 3,540,000	ESA, EXPOSE-R G. Horneck, DLR; D. Häder, UE; Ts. Dachev, SRTI. (Dachev, 2013a) (Dachev et al., 2015a) Bulgaria, Germany	R3DR 1 DU ($76 \times 76 \times 36$ mm, 0.19 kg) Outside of the ISS in the EXPOSE-E facility outside of the Zvezda module $>0.6 \text{ g cm}^{-2}$; 10 s	 	
12	Phobos-Grunt 09/11/2011 (The satellite was lost because of rocket booster malfunctioning)	Liulin-Phobos V. Petrov, IMBP; J. Semkova, SRTI. (Semkova et al., 2008). Bulgaria, Russia	Liulin-Phobos 2 × 2 dosimetric telescopes ($172 \times 114 \times 45$ mm 0.5 kg) Outside the Phobos-Grunt satellite; $>2 \text{ g cm}^{-2}$ Dose and flux 60 s Spectrum 60 min	 	

(continued on next page)

Table 1 (continued)

Part 2					
Item No.	Satellite	Experiment name	Instrument Size [mm]/Mass [kg]	Instrument location image	External view of the instrument
	Date begin–Date end	PI CoPI	Place Shielding [g cm^{-2}] Resolution [s]/[min]		
	Available number of measurements	References Cooperation			
13	"BION-M" No. 1	RD3-B3	RD3-B3		
	19/04/2013– 13.05.2013	V. Shurshakov, IMBP; Ts. Dachev, SRTI	(110 × 80 × 44 mm, 0.3 kg)		
	In space 34,391 spectra	(Dachev et al., 2015b) Bulgaria, Russia, Germany	1 battery operated DU Inside the "BION-M" No. 1 satellite/ $>2 \text{ g cm}^{-2}$; 60 s		
14	"Foton-M" No. 4	RD3-B3	RD3-B3		
	18/07/2014– 01.09.2014	V. Shurshakov, IMBP; Ts. Dachev, SRTI	(110 × 80 × 44 mm, 0.3 kg)		
	In space 64,109 spectra	Bulgaria, Russia, Germany	1 battery operated DU Inside the "Foton-M" No. 1 satellite/ $>2 \text{ g cm}^{-2}$; 60 s		

monaut, which was supported by the Bulgarian and former USSR governments and was the product of wide-ranging conversations and competition concerning the type of instruments to be developed and built for the mission on the MIR space station. In conversation, in 1986, with Dr. M.V. Tel'tsov (one of the developers of the R-16 instrument from the Skobeltsyn Institute of Nuclear Physics of Moscow State University) we were advised that a small active personal dosimeter the size of a wrist watch was very necessary and would be supported by the selection commission of the program. This was the initial impetus for the development of the Liulin instruments. We contacted colleagues from the Institute of Biomedical Problems, Russian Academy of Sciences, Moscow, Russia and on the basis of their experience (Markelov and Redko, 1981) the first Liulin was developed between 1986 and 1988 (Dachev et al., 1989). Today's Liulin devices are more than 100 times lighter and consume less than 1000 times the power of the first device (but still aren't the size of a wrist watch).

All Liulin-type dosimetric instruments use one or more silicon detectors and measure the deposited energy and number of particles in the detector(s) when charged particles hit the device, allowing it to calculate the dose rate and particle flux.

The measurements in the original LIULIN instrument were based on a single silicon detector followed by a charge-sensitive shaping amplifier (CSA). The number of the pulses at the output of CSA above a given threshold was proportional to the particle flux hitting the detector; the amplitude of the pulses at the output of the CSA was proportional to the particles' deposited energy, and the integral of the energy depositions of the particles accumulated in the detector during the measurement interval allowed calculation of the dose rate. Using the opportunity provided by Dr. J. Miller of Lawrence Berkeley National Laboratory, Berkeley, USA, post-flight calibrations of the LIULIN detector that had flown in space were performed with 1 GeV nucleon⁻¹ ^{56}Fe ions at the Brookhaven National Laboratory AGS accelerator (Dachev et al., 198a).

The RADIUS-MD instrument (see Table 1, Part 1, Item No. 2) used the same measurement procedure as the LIULIN instrument. It was developed and qualified for space together with French and Russian colleagues for the unsuccessful Mars-96 mission (Semkova

et al., 1994). The LIULIN and RADIUS-MD instruments were designed to provide data only for the dose rate and particle flux in a single detector, but not the deposited energy spectrum. This design was later abandoned, and we will not describe it here, but will summarize the major results obtained during the operation of the LIULIN instrument on the MIR space station between June 1988 and September 1994.

Many other instruments have since been developed and used in space, on the ground, in aircraft and on balloons. This paper aims to review the major milestones of their development, calibration and scientific results.

Table 1 summarizes information for all instruments developed and built in Bulgaria that have been used in the near Earth radiation environment or around the Moon.

A total of 14 different space instruments were developed and qualified for space between 1988 and 2014. Three of them were lost because of problems with the rockets of the Mars-96, Foton-M1 and Phobos-Grunt missions. The R3D-B1 instrument for the Foton-M1 mission is not shown in the table because it was very similar to the R3D-B2/B3 instruments for the Foton-M2/M3 missions.

The first column in Table 1 shows the name of the satellite, start and end time of the experiment and the number of available measurements. The second column lists the name of the experiment, the principal investigator (PI), Co-PIs and countries involved. Major references describing the instrument and data obtained are also listed. The third column gives the name of the instrument, technical specifications, location, shielding and time resolution of the instrument. The last two columns show images of the instruments and their locations (carriers).

2.1. DES instrumentation

2.1.1. DES description

The main purpose of the Liulin type Deposited Energy Spectrometer (DES) is to measure the deposited energy spectrum (in 256 channels) in a silicon detector from primary and secondary particles at aircraft and balloon altitudes, in LEO, and outside the

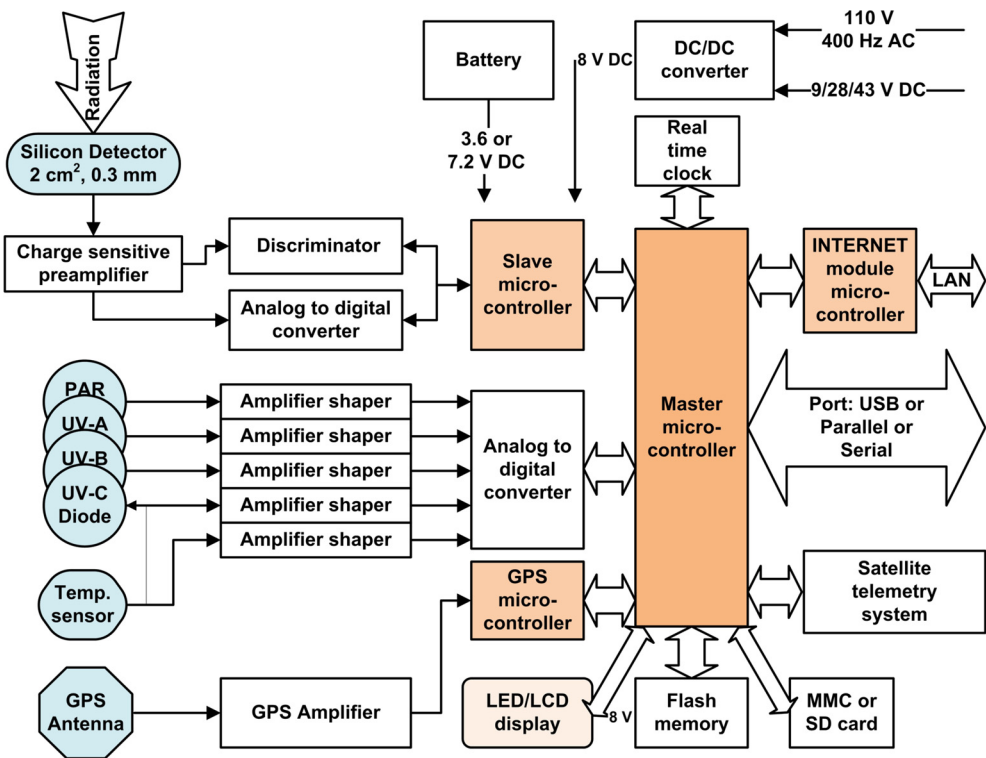


Fig. 1. Generalized block diagram of Liulin-type DES instruments.

geomagnetosphere en route, around and on the surface of the planets in the solar system.

Historically the first development of a DES was for the Liulin-3M instrument ([Dachev et al., 2003](#)) for use on aircraft and balloons ([Stassinopoulos et al., 2002](#)) and for BION-11/12 missions. Later versions of the Liulin-3M instrument were Liulin-4 and Liulin-6 (which are synonymous with DES). The Liulin-4 type instrument was developed in cooperation with Dr. R. Beaujean and partially supported by a contract in 1996 between the Solar-Terrestrial Influences Laboratory at the Bulgarian Academy of Sciences (STIL-BAS) and the Rektorat der Christian-Albrechts-Universitaet zu Kiel.

[Fig. 1](#) presents a generalized block diagram of a Liulin-type DES ([Dachev et al., 2011a](#)). A DES usually contains: one semiconductor detector, one charge-sensitive preamplifier, a fast 256 channel analog-to-digital converter (ADC), discriminator, real time clock, two or more microcontrollers and a flash memory. Different modifications of DESs use additional modules such as: UV sensitive photodiodes, a temperature sensor, a Global Positioning System (GPS) module with antenna and receiver, LED or LCD display, multimedia card (MMC) or SD card.

A pulse analysis technique is used to obtain the deposited energy from each photon/particle partially or fully crossing the silicon detector. The deposited energies recorded in 256 channels form the deposited energy spectrum for each measurement cycle. It is used in addition for the calculation of the absorbed dose and flux in the silicon detector from primary and secondary particles. Analysis of the shape of the spectrum and the dose to flux ratio, known also as specific dose (SD), permits the characterization of the predominant radiation source in the DES environment ([Dachev, 2009](#)).

The unit is managed by microcontrollers through specially developed firmware. The ADC and the slave microcontroller organize the deposited energy spectrum in 256 channels and store it in RAM memory. The master microcontroller (seen in the right part of [Fig. 1](#)) manages the whole operation of the spectrometer and data

outputs. The modifications permit storing the spectrum data in a flash memory or on an SD/MMC card, transmission of the spectra data to a parallel, serial or USB port, transmission of spectra data to a web module and further to a LAN network, and dose and flux data visualization on an alphanumeric or graphic display.

For the two R3D-B2/B3 instruments on Foton satellites and for the R3DE/R instruments on ISS (see [Table 1](#), Part 1, Item No. 4/7 and Part 2 Item No. 9/11), 4 photodiodes with filters at different wavelengths and 1 temperature input channel were added to the system using the schematics developed by colleagues from the University of Erlangen, Germany ([Streb et al., 2002](#)).

Another type of input is the GPS tract, which consists of GPS antenna, receiver and microcontroller unit (MCU). This is used by aircraft instruments for positioning of the measurements by the geographic longitude, latitude, altitude above sea level and Universal Time (UT) ([Green et al., 2005; Getley et al., 2010; Hwang et al., 2010](#)).

Different power supplies were used in the different instruments. They are presented in the upper part of [Fig. 1](#) and include 3.6 V or 7.2 V rechargeable or primary batteries, 28 V or 43 V DC aircraft and satellite power or 110 V, 400 Hz AC aircraft power line.

The main measured parameter in the DES is the amplitude of the pulse after the CSA, generated by a particle or a photon partially or fully crossing the detector ([Dachev et al., 2002](#)). The amplitude of the pulse is proportional by a factor of 240 mV MeV⁻¹ to the energy deposited in the detector and to the dose, respectively. These amplitudes are digitized in an 8-bit ADC and organized in a 256-channel deposited energy spectrum.

By definition the dose in the silicon detector D_{Si} [Gy] is one joule deposited in 1 kg of matter. The DES absorbed dose is calculated by dividing the summarized energy deposition in the spectrum in joules by the mass of the detector in kilograms:

$$D_{Si} \text{ [Gy]} = K \sum_{i=1}^{255} (EL_i i) [\text{J}] / MD [\text{kg}] \quad (1)$$

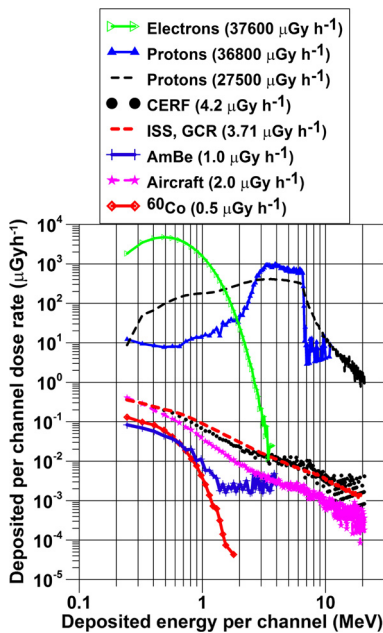


Fig. 2. Different spectral shapes obtained by Liulin-type instruments during calibrations and on aircraft and spacecraft.

where K is a coefficient. MD is the mass of the detector, and EL_i is the energy loss in Joules in channel i . The energy in MeV is proportional to the amplitude A of the pulse: EL_i [MeV] = A [V]/0.24 [V/MeV], where 0.24 [V/MeV] is a coefficient dependent on the preamplifier used and its sensitivity.

All 255 deposited dose values, depending on the deposited energy for one exposure period, form the deposited energy spectrum. Channel 256 accumulates all pulses with amplitudes higher than the upper energy of 20.83 MeV measured by the spectrometer. The methods for characterization of the type of incoming space radiation are described in Dachev (2009) and Dachev et al. (2011b).

2.1.2. DES calibrations

Fig. 2 shows deposited energy spectra from different calibrations of the DES, which are compared with experimental proton, electron and GCR spectra obtained at aircraft altitudes and on spacecraft. The individual spectra seen in the figure are obtained after averaging various numbers of primary spectra and are plotted in coordinates as deposited energy per channel/deposited per channel dose rate. This allows a better understanding of the process of formation of the spectra in different deposited energy ranges. According to Eq. (1) the absorbed dose in Si is the area between the curve of the deposited energy spectrum and the abscissa. That is why from bottom to top each spectra position against the ordinate axes depends on the value of the deposited dose rates in Si seen in the legend at the top of the figure. The higher the measured dose rate, the higher the position of the spectrum against the ordinate axis, and the greater the area between the spectrum and the abscissa.

The lowest line spectrum in Fig. 2 ($D = 0.5 \mu\text{Gy h}^{-1}$, diamond) was obtained by Prof. Frantisek Spurny during the calibration of the Liulin-4C Mobile Dosimetry Unit MDU#2 (see Table 2, Item No. 1) with ^{60}Co as a reference radiation source at the Nuclear Physics Institute of the Czech Academy of Sciences (Spurny and Dachev, 2003). This spectrum is the shortest because the energy of the ^{60}Co gamma emission line is 1.2 MeV. The absolute values of the dose rates obtained from the spectra are in very good agreement with the dose rates calculated using the EGS4 transport code (<http://rcwww.kek.jp/research/egs/>). The values of the measured doses were found to be within 2.8% of the reference value

for the ^{137}Cs source and within 8% of the ^{60}Co source (Spurny and Dachev, 2003). The calibrations showed that the DES had high effectiveness with respect to gamma rays, which allowed monitoring of the natural background radiation.

The spectrum denoted by crosses in Fig. 2 was generated by a reference AmBe radiation source emitting neutrons with an average energy of 4.4 MeV. This spectrum continues up to about 4 MeV deposited energy with an obvious change in the slope around 1.2 MeV deposited energy. The neutron sensitivity of the DES was further studied in the CERN-EU high-energy reference field (CERF) facility (Mitaroff and Silari, 2002), on aircraft and in the near Earth radiation environment. The spectrum with heavy dots in Fig. 2 obtained in the CERF facility field contains events in all channels of the DES including the 256th channel, devoted to energy depositions above the upper level of the spectrometer at 20.83 MeV. The events seen below 1 MeV in AmBe and at CERF represent the contribution of low LET radiation (electrons, muons, etc.), while the events above 1 MeV represent the high LET components (protons, neutrons and ions heavier than H). This idea was further developed and allowed calculation of the ambient dose equivalent $H^*(10)$ at aircraft altitudes from the deposited energy spectrum in the silicon detector (Spurny, 2005; Green et al., 2005; Ploc et al., 2011; Kubančák et al., 2014).

The CERF energy deposition spectrum is very similar to the averaged aircraft spectrum shown with asterisks in Fig. 2. This spectrum is obtained by averaging Czech Airlines aircraft data during mean solar activity at altitudes close to 10.6 km on routes between Prague and the North American cities New York and Montreal (Spurny et al., 2009). The ISS R3DE instrument (see Table 2, Item No. 5) mean GCR deposited energy spectrum (heavy dashed line) has a shape even closer to the CERF spectrum. The spectrum was obtained by the R3DE instrument outside the ISS by averaging all measurements with 10-s resolution for 2418 h in the period 20 February–31 December 2008 (Dachev et al., 2012a).

CERF, ISS and aircraft spectra in Fig. 2 show a similar knee around 6.5–7 MeV deposited energy. To explain this knee in Fig. 2 a spectrum ($36800 \mu\text{Gy h}^{-1}$) (heavy triangles) was added to the figure. This was obtained during calibrations of DES (non-shielded detector) with a 7.8 MeV protons beam at the cyclotron facility of the University of Louvain, Belgium (Dachev et al., 2002). The knee seen at about 6.3 MeV corresponds to the point where the incident energy of the normally incident beam on a 0.3 mm thick detector is equal to the deposited energy. All normally incident protons with energies less than 6.3 MeV are stopped in the detector. The exact value of the incident energy at which the CSDA (continuous-slowing-down approximation) range in silicon is 0.3 mm is 6.04 MeV (Berger et al., 2014).

The light dashed spectrum in Fig. 2 with 27.5 mGy h^{-1} absorbed dose rate was obtained by the RADOM instrument (see Table 1, Part 2, Item No. 10) on the Chandrayaan-1 satellite by averaging of 60 primary 10-s resolution spectra (Dachev et al., 2011c). This spectrum shows a very similar shape to the cyclotron facility spectrum ($36800 \mu\text{Gy h}^{-1}$ full triangle spectrum) and a knee at the same position. This is because the energy of the inner belt protons falling on the detector is calculated to be 7–8 MeV, i.e. equal to the energy of the cyclotron facility's monoenergetic protons falling on the non-shielded detector. The main differences between the spectra are seen in the deposited energy range 0.244–2.8 MeV where a large number of low LET particles and electrons are observed. The smaller slope of the space spectrum after the knee can be explained by the presence in space of additional ions heavier than protons.

The open triangle spectrum is the highest one in Fig. 2. It was obtained on the Chandrayaan-1 satellite at altitudes of the ORB (22 000 km). This spectrum with a predominant electron population is the result of averaging 120 spectra with 10-s resolution.

Table 2

Liulin type experiments at aircraft, balloon, rocket and mountains peaks.

Item No.	Experiment description Date begin–Date end	Person performing the experiment References	Instrument Size [mm]/Mass [kg] Place Resolution [s]	External view of the instrument
1	1. Balloon experiment at Gap-Tallard aerodrome, France, 14/06/2000; 2. NASA's Lockheed ER-2 high altitude research aircraft, Oct.–Nov. 2000.	1. CNES balloon technological flight program, F. Spurny, NPI-CAS, Prague, Czech Republic; 2. Y. Uchihori, NIRS, Japan; (Spurny, 2000) (Uchihori et al., 2003c)	Liulin-4C/4J, MDU-2 (100 × 64 × 24 mm, 0.23 kg with rechargeable Li-Ion battery pack) Inside of the balloon gondola or the ER-2 cockpit, 60 s	
2	Long-term (>60 days) measurements at aircraft altitudes for different airlines. 28 V DC/DC converter. Since 2001 up to 2014.	F. Spurny and O. Ploc, NPI, Czech Rep; (Ploc et al., 2013). J.C. Saez Vergara and R. Dominguez-Mompell Roman, CIEMAT and IBERIA, Spain. (Hwang et al., 2010), KASI, Korea	DU (110 × 100 × 45 mm, 0.48 kg including 2 D size Lithium-Ion batteries) Inside of the aircraft 300/600 s	
3	Deep Space Test Bed (DSTB) certification flight 8 June 2005 at Ft. Sumner, New Mexico, USA. ~10 h	E.R. Benton, ERIL Research Inc. & Y. Uchihori, NIRS, Japan; (Benton, 2005a, 2005b) http://wrmis.org/workshops/tenth/pdf/08_benton.pdf	3 Liulin MDU (100 × 64 × 24 mm, 0.23 kg with rechargeable Li-Ion battery pack) Inside of the balloon gondola 60 s	
4	Measurements at mountain peaks. The Liulin instrument contains Internet module to post, store and transmit the obtained results via FTP protocol in Internet.	Bern University, Jungfrau, Switzerland: http://130.92.231.184/ Lomnitski Shtit: http://147.213.218.13/ INRNE-BAS, BEO-Moussala: http://beo-db.inrne.bas.bg/moussala/	DU (84 × 40 × 40 mm, 0.12 kg). Internet module with 22 MHz microprocessor, 512 KB flash and 512K SRAM memory. 600 s	
5	Measurements at aircraft altitudes. A built in GPS receiver record: UT, Longitude, Latitude and Altitude, which together with the dose rate data are shown on the display.	I. Getley, University of New South Wales, Australia (Getley et al., 2010)	Spectrometer (110 × 55 × 45 mm; 0.38 kg); Display (115 × 40 × 20 mm; weight 0.12 kg; Rechargeable battery package (90 × 60 × 40 mm; 0.18 kg). Inside of the cockpit of Boeing 747-400 Qantas Airways flights. 60 s	
6	1. NASA balloon experiment for radiation studies. 2. RAZREZ system on ISS (The both systems are already delivered but both exp. are not performed.)	1. (Adams et al., 2007) NASA/Marshall Space Flight Center, USA. 2. (Petrov et al., 2010) http://wrmis.org/workshops/fourteenth/Petrov.pdf	4 DU (74 × 40 × 20 mm, 0.065 kg; 1 CIU (144 × 60 × 20 mm, 0.21 kg) Total 0.47 kg. Powered from 28 V DC, 0.72 mA. Data transmission through RS485 interface.	
7	Under the HotPay2 project from Andoya Rocket Range, Norway was launched a rocket up to 380 km altitude on January 31, 2008.	(Tomov et al., 2008) http://www.stiil.bas.bg/FSR/PDF/TOP5Tomov_Borislav2242058.pdf	(110 × 40 × 20 mm, 0.098 kg) Inside of the rocket payload 60 s	

(continued on next page)

Table 2 (continued)

Item No.	Experiment description Date begin–Date end	Person performing the experiment References	Instrument Size [mm]/Mass [kg] Place Resolution [s]	External view of the instrument
8	5 balloon flights up to 30 km altitude between July 2011 and August 2012	Physikalisch-Technische Bundesanstalt (PTB), Germany (Wissmann et al., 2013)	Liulin-RG4/5 2 DU (110 × 40 × 20 mm 0.092 kg). With serial readout of the data measured with the Si-detector. On the gondola of the balloon. 30 s	
9	Long-term (>60 days) measurements at aircraft balloon altitudes. A built in GPS receiver record: UT, Longitude, Latitude and Altitude. Data are stored at 1 or 2 GB SD card. 28 V DC/DC converter. Since 2005 up to 2014.	Royal Military College of Canada, Canada, PTB, Germany (Wissmann et al., 2013) (Green et al., 2005) (Kitching, 2004)	Liulin-66SG 1 DU (110 × 100 × 45 mm, 0.48 kg including 2 D size Lithium-Ion batteries) Inside of the aircraft or on the gondola of the balloon 30/300/600 s	

Only the part with deposited energies up to 4.0 MeV is shown. The spectrum continues with a shape similar to the ISS GCR spectrum (shown with thick line without symbols in Fig. 2) but here the incoming GCR particles are not well detected because of the very high count rate of the spectrometer and consequently large dead time.

The exact position of the knee depends on the thickness of the detector shielding and on the exact detector thickness, which are different for different instruments. The larger these values are, the larger is the value of the knee in the spectrum. That is why in Fig. 2 the knee is observed above the calculated value of 6.04 MeV ([Berger et al., 2014](#)) in the range 6.0–7.0 MeV. The average value of 6.2 MeV deposited energy corresponds to channel number 78, which means that all other channels up to 256 of the spectrometer are populated by long pathlength low LET particles (protons) or by neutrons and heavier ions.

A more comprehensive description of the DES calibrations with protons in the Louvain la-Neuve cyclotron facility is presented in [Dachev et al. \(2002\)](#). [Uchihori et al. \(2002\)](#) performed calibrations with protons and heavy ions at the Heavy Ion Accelerator at the National Institute of Radiological Sciences (NIRS) facility in Chiba, Japan (HIMAC). In both proton calibrations good agreement was found between the measured spectra and those predicted by the GEANT-4 code (<http://geant4.cern.ch/>). Good agreement was also found between predictions and measurements obtained by Liulin-4J (MDU-3) of the response function as reported by [Uchihori et al. \(2003a\)](#) (see their Fig. 2). The response function was accumulated by points obtained in H⁺, He⁺, C⁺ (400 MeV) and Ca⁺ (400 MeV) beams.

The DES effectiveness for neutrons depends on their energy, being minimal for neutrons with an energy of 0.5 MeV and having a maximum of a few percent for neutrons with energies of 50 MeV in the CERN field ([Spurny, 2005](#)). According to the “neutron induced nuclear counter effect” introduced for the Hamamatsu PIN diodes of type S2744-08 ([Zhang et al., 2011](#)) almost all DESs used the same type PIN diodes and neutrons could be observed in all channels of the spectrum with a probability at least one order of magnitude higher in the first 14 channels.

2.1.3. DES data intercomparison with other instruments data

Post-flight calibrations with Liulin-E094 MDUs (see Table 1, Part 1, Item No. 3) were performed at the HIMAC heavy ion accel-

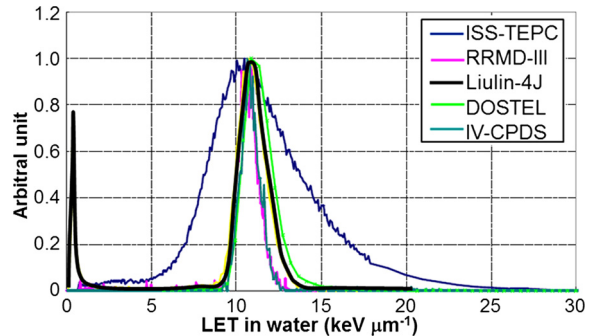


Fig. 3. Comparison of the deposited energy spectra obtained by the Liulin-4J instrument with another three Si telescopes and ISS-TEPC, obtained during the ICCHIBAN-1 test run with 400 MeV/u carbon ions.

erator during the 1st ICCHIBAN (Inter Comparison for Cosmic-ray with Heavy Ion Beams At NIRS) Project, run in Chiba Japan in February 2002 with 400 MeV/u carbon ions. The deposited energy spectra obtained with all 4 MDUs show a sharp maximum close to 6.1 MeV in good agreement with the theoretical prediction and with measurements of the same source with the DOSTEL-1 instrument ([Burmeister et al., 2003](#)).

Fig. 3 shows a comparison of the deposited energy spectra obtained by the Liulin-4J instrument (see Table 2, Item No. 2) with three other silicon telescopes (RRMD-III, DOSTEL, IV-CPDS) and the ISS-TEPC obtained during the ICCHIBAN-1 runs with 400 MeV/u carbon ions ([Uchihori et al., 2003b](#)). The silicon detector results for the LET spectrum are in good agreement. The ISS-TEPC spectrum is broader, owing to the instrument structure (chord length distribution).

For purposes of in-flight intercomparison between Liulin data with data from another instrument Fig. 4 contains data from the tissue equivalent proportional counter (TEPC) and two Liulin DES instruments – R3DE/R (see Table 1, Part 2, Item Nos. 9 and 11). The TEPC data are plotted in Fig. 4 using the opportunity provided by [Zapp \(2013\)](#) and by the ‘Coordinated Data Analysis Web’ at the NASA-Goddard Space Flight Center (<http://cdaweb.gsfc.nasa.gov/>).

The dose rate data presented in Fig. 4 are plotted versus the UT and show three passes across the SAA region denoted by labels SAA1–SAA3, seven passes across the high latitude GCR regions

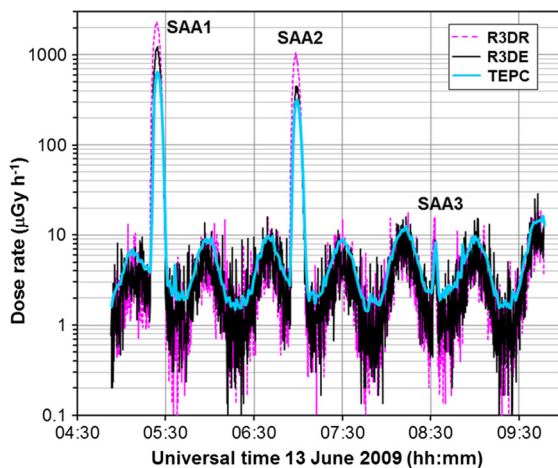


Fig. 4. Comparison of the dose rates measured simultaneously by the R3DE/R instruments and the NASA TEPC for the period 4:53–9:46 UT on 13 June 2009.

in both hemispheres and six passes across the magnetic equator. Analysis of the dose rate dynamics in Fig. 4 shows the following: 1) The R3DR SAA dose rates are the highest and reach $2304 \mu\text{Gy h}^{-1}$ during the SAA1 maximum because the R3DR is the most lightly shielded instrument (Dachev, 2013a). The more heavily shielded (by surrounding masses) R3DE dose rates are about half of that ($1222 \mu\text{Gy h}^{-1}$), whereas the TEPC dose rates (heaviest shielded inside the ISS) are the smallest ($645 \mu\text{Gy h}^{-1}$). 2) The TEPC dose rates are higher than the R3DE/R dose rates because the TEPC is sensitive to a much higher LET range (up to $\sim 1000 \text{ keV } \mu^{-1}$ in tissue); thus, the TEPC can measure dose from all the heavy-ions in the GCR spectrum. In the regions of the magnetic equator the lowest dose rate values are obtained by the R3DR instrument. The R3DE dose rates are in the middle, whereas the TEPC dose rates are the highest. The doses accumulated by the three instruments for 4 h and 56 min are respectively 261 μGy (R3DR), 132 μGy (R3DE) and 100 μGy (TEPC).

DES intercomparison of dose rate measurements on aircraft has been performed in many cases. Here we report some of the more significant ones. The exposure of aircraft crew to cosmic radiation has received a great deal of attention since the recommendation by the International Commission on Radiological Protection (ICRP) in 1990, that exposure to cosmic radiation in the operation of jet aircraft should be recognized as occupational exposure, which spurred a number of new dose measurements on board aircraft (Radiation Protection 140, 2004). The cited report contains many of the DES dose rate measurements performed by Prof. Frantisek Spurny and comparisons with other instruments and computer codes confirms the capability of DES to characterize the radiation field at aircraft altitudes.

The response of a LIULIN-4 spectrometer was compared by Green et al. (2005) to that of the HAWK TEPC <http://www.fwt.com/detector/fw-ad1ds.htm> on 42 aircraft flights in 2003–2004 covering the full range of cutoff rigidity values. On all flights the absorbed dose measured by both instruments agreed to within 5%. These data provided an in-flight validation of the calibration factor determined by us in ground-based studies.

Getley et al. (2010) performed intercomparison measurements with different detectors including a TEPC and Liulin-4SA (see Table 2, Item No. 5) on board Boeing 747-400 Qantas Airways flights between August 2008 and March 2009. The flight routes involved cross-equatorial flights between Sydney, Melbourne and Los Angeles. A northern latitude flight traveled between Sydney, Hong Kong, London and Singapore, and numerous high southern latitude flights were flown between Sydney and Johannesburg and Sydney and Buenos Aires. In the summary of the paper they wrote: “Com-

prehensive testing of both the Liulin and QinetiQ QDOS/Rayhound over a 6 month period, at both high northern and southern latitudes as well as in cross-equatorial flights, suggests that both of these spectrometers have the ability to provide reliable dose assessments for aircrew monitoring.”

The containers and additional materials of most of the DES instruments described in this paper provide between 0.41 and 0.6 g cm^{-2} shielding. For the lower boundary of 0.41 g cm^{-2} shielding the calculated stopping energy of normally incident particles to the detector is 0.78 MeV for electrons and 15.8 MeV for protons (Berger et al., 2014). For 0.6 g cm^{-2} shielding these values are 1.18 MeV for electrons and 27.5 MeV for protons. This means that only protons and electrons with energies higher than the values listed above can reach the instrument detector.

2.2. Dosimetric telescope (DT) instrumentation

2.2.1. DT description

The first application of the Liulin DT method was for the Liulin-5 instrument on ISS. Liulin-5 (see Table 1, Part 1, Item No. 6) was an active instrument in a spherical phantom (Semkova et al., 2007). The aim of the Liulin-5 experiment was to make a long-term investigation of the depth-dose distribution and continuous monitoring of the particle fluxes, dose rates, energy deposition and LET spectra in a radial channel of the Russian spherical tissue-equivalent phantom MATROSHKA-R (Akatov et al., 2002; Shurshakov et al., 2006), using a telescope of three silicon detectors. Liulin-5 is sensitive to photons, electrons, protons and heavy ions. A Liulin-5 charged particle telescope was launched to the ISS by the Progress-60 cargo craft in May 2007.

Investigation of the radiation environment in the phantom on the ISS by the Lulin-5 experiment comprised: 1) measurement of the depth distributions of the energy deposition spectra, flux and dose rate and absorbed dose D ; 2) measurement of the LET spectrum in silicon and then calculation of the LET spectrum in water and Q , according to the $Q(L)$ relationship given in ICRP-60, where L stands for LET. $Q(L)$ is functionally related to the unrestricted LET of a given radiation and is multiplied by the absorbed dose to derive the dose equivalent H . H , D and Q are related by:

$$H = Q_{\text{ave}} D, \quad (2)$$

where D is the absorbed (integrated over all particles) dose, and Q_{ave} is the dose averaged quality factor, given by:

$$Q_{\text{ave}} = \int Q(L) D(L) dL / D \quad (3)$$

The Liulin-5 instrument consists of two units: a detector module and an electronics module (see Table 1, Part 1, Item No. 6). The detector module is mounted in the radial channel of the phantom, while the electronics are outside of the phantom. A more detailed description of the Liulin-5 method and instrument can be found in Semkova et al. (2007, 2010). The detector module contains 3 silicon detectors (D1–D3) arranged as a particle telescope. Fig. 5 is a schematic diagram of the Liulin-5 in the spherical phantom. The sensitive thickness of the detectors D1 and D3 is 370 μm , of D2, 360 μm and the detectors' diameter is 17.2 mm. The D1 detector is placed at 40 mm depth in the phantom, D2 is at 60 mm and D3 is at 165 mm distance from its surface.

From each detector the energy deposition spectrum for a measurement cycle is recorded in two 256 channel sub-ranges. Then the overall energy deposition spectrum is constructed in 512 channels. The energy ΔE deposited in the detector is proportional to the value $k_1 \sum (iN_i) + k_2 \sum (jN_j)$, and the incident particle flux is proportional to $\sum N_i + \sum N_j$. Here i and j are the spectral channel numbers in the two sub-ranges (lowLET and highLET), N_i and N_j are the amounts of particles registered in channels i and j of the

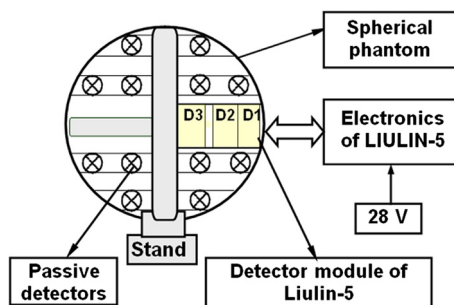


Fig. 5. Schematic diagram of the Liulin-5 experiment in the spherical phantom.

corresponding sub-ranges, and k_1 and k_2 are normalization coefficients. The values $\sum(iN_i)$, $\sum(jN_j)$, $\sum N_i$, $\sum N_j$ are recorded for given time intervals and are used for calculation of the doses and particle fluxes rates.

The absorbed dose in the detector is calculated as

$$D = \Delta E/m, \quad (4)$$

where m is the mass of the detector.

The geometry factor for converting the measured number of particles in a single detector into a differential flux is $14.6 \text{ cm}^2 \text{ sr}$, assuming the incident flux is isotropic.

Detectors D1 and D2 operate in coincidence mode. The distance between D1 and D2 is 20 mm and the viewing angle of the D1–D2 assembly is 81.4 degrees. When a particle enters the telescope within the 81.4-degree sensitivity cone with an energy high enough to make it through both the D1 and D2 detectors, it is considered a coincident event. The energy deposition spectrum measured in the D1 detector in coincidence mode with D2 is recorded and used to obtain the LET spectrum. Since the incidence angle of the particles is not measured, the energy deposition is converted into a mean LET in silicon as:

$$\text{LET}(\text{Si}_i) = \Delta E_i/h_{D1}, \quad (5)$$

where ΔE_i is the deposited energy in channel i , $\text{LET}(\text{Si}_i)$ is the LET in silicon in channel i (here i is from 1 to 512) and h_{D1} is the thickness of D1. Calculations show that the dependence of the effective area of the telescope on the particle incident angle is practically linear and decreases from 2.324 cm^2 at 0° between the telescope axis and flux to 0 cm^2 at 40.7° . The average increase of the particle range in the detector in the case of incidence not parallel to the axis is 7%.

The LET spectra in silicon are used for calculation of the differential and integral LET spectra in water, the absorbed dose rates and the quality factors. The geometry factor for converting the measured amount of particles by the D1–D2 telescope into differential isotropically incident flux is $2.01 \text{ cm}^2 \text{ sr}$. The energy deposition in water (a surrogate for tissue) relative to that in silicon is taken to be 1.24, assuming no dependence on particle energy. LET in water $\text{LET}(\text{H}_2\text{O})$ is then found by the following relation:

$$\text{LET}(\text{H}_2\text{O}) = 1.24 \times \text{LET}(\text{Si})/2.34 \quad (6)$$

Taking into account that the relation between $\text{LET}(\text{H}_2\text{O})$ and $\text{LET}(\text{Si})$ changes with proton energy E_p from 1.27 for $E_p = 30 \text{ MeV}$ to 1.21 for $E_p = 1000 \text{ MeV}$ and that for a typical energy $E_p = 100 \text{ MeV}$ the conversion coefficient is 1.24, the maximum difference of $\text{LET}(\text{H}_2\text{O})$ obtained by using a real conversion function and the simple conversion factor is less than 3%.

To obtain the dose of the isotropically incident particles from the dose measured by the D1–D2 telescope, the dose calculated from the D1–D2 coincidence spectrum is multiplied by a correction coefficient of 13.5.

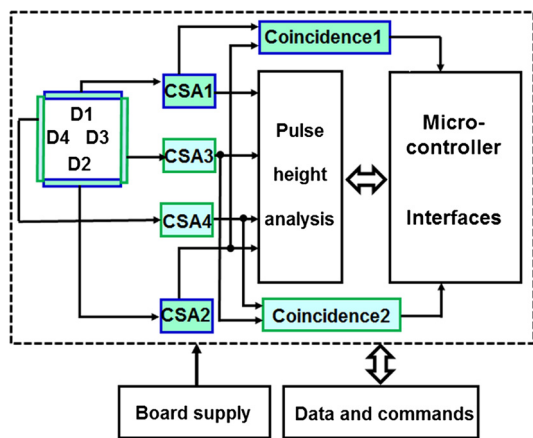


Fig. 6. Block schematic of the Liulin-Phobos charged particle telescope.

The instrument provides in a time-resolved manner: absorbed dose rate in each detector, flux rate in the range $0-4 \times 10^2 \text{ cm}^2 \text{ s}^{-1}$, measured in each detector, energy deposition spectra in the D1 detector in the range $0.45-63 \text{ MeV}$ in 512 spectral channels, energy deposition spectra in the D2 detector in the range $0.45-60 \text{ MeV}$ in 512 spectral channels, energy deposition spectra in the D3 detector in the range $0.2-10 \text{ MeV}$ in 512 spectral channels, $\text{LET}(\text{H}_2\text{O})$ spectra in the range $0.65-90 \text{ keV } \mu\text{m}^{-1}$ in 512 spectral channels. The events exceeding the upper energy deposition or LET limit of each detector are recorded in the corresponding 512 channel.

The second application of the DT method was for the Liulin-Phobos instrument (see Table 1, Part 2, Item No. 12) developed for the Phobos-Grunt mission (Semkova et al., 2008). The main goal of the Liulin-Phobos experiment was the investigation of the radiation environment and doses in the heliosphere at distances of 1 to 1.5 AU from the Sun and in the near-Mars space.

The Liulin-Phobos instrument consisted of two dosimetric telescopes, D1&D2 and D3&D4, arranged in two perpendicular directions. The block schematic of the instrument is shown in Fig. 6. Each pair of telescopes consists of two 0.3 mm thick Si PIN photodiodes, operating in coincidence mode to obtain the LET. One of the detectors in every telescope measures the energy deposition spectrum in the range $0.1-10 \text{ MeV}$ and the other in the range $0.45-90 \text{ MeV}$. In that way each dosimetric telescope provides data in the energy deposition range $0.1-90 \text{ MeV}$. The instrument was designed to measure absorbed dose rate and particle flux every 60 s, and energy deposition spectra and LET spectrum every 60 min.

The data taken by the Liulin-Phobos DT were: absorbed dose rate in the range $4 \times 10^{-8}-0.1 \text{ Gy h}^{-1}$ and absorbed dose D , measured by every single detector, particle flux in the range $0-10^4 \text{ cm}^{-2} \text{ s}^{-1}$, measured by each detector, energy deposition spectra in the range $0.1-90 \text{ MeV}$, measured by each dosimetric telescope, LET spectrum (in H_2O) in the range $0.75-155 \text{ keV}/\mu\text{m}$, measured by each DT, quality factor $Q = f(\text{LET})$ and average quality factor Q_{ave} , dose equivalents $H = Q_{\text{ave}}D$, measured by two DTs.

An instrument similar to the Liulin-Phobos DT is now under development for the ExoMars mission (Dachev et al., 2013a).

2.2.2. DT calibrations

Liulin-5 was exposed to $400 \text{ MeV/n}^{16}\text{O}$ and $300 \text{ MeV/n}^{56}\text{Fe}$ beams during the ICCHIBAN-7 experiments (Uchihori et al., 2005) at HIMAC in September 2005.

Fig. 7 shows the deposited energy distribution in the silicon detectors of Liulin-5 obtained during the exposures to $400 \text{ MeV/n}^{16}\text{O}$ (Semkova et al., 2007). The detector module of Liulin-5 was first exposed perpendicular to the beam with a beam center at the

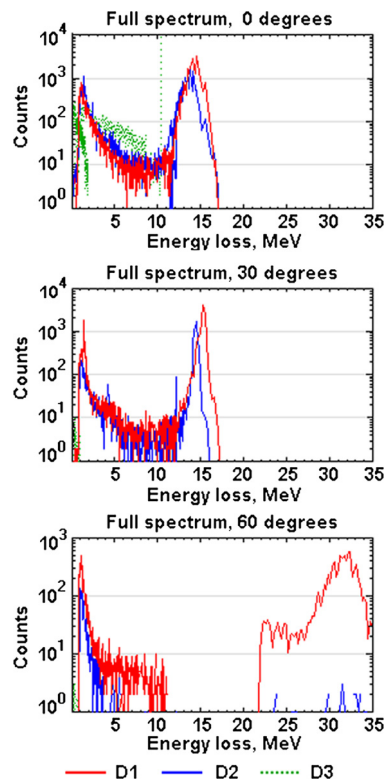


Fig. 7. Energy deposition distributions of the ^{16}O beam in the silicon detectors D1–D3 of Liulin-5.

center of the detectors (0° inclination). Next, the detector module of Liulin-5 was inclined by angles of 30° and 60° relative to the beam line and rotation measurements were made around the center of D1 detector.

On each plot two distributions are seen – the left represents measured spectra in the low-LET range and the right represents measured spectra in the high-LET range of the detectors. We assume that the high-LET peaks correspond to the distribution of the main ^{16}O beam, and the low-LET peaks correspond to scattered background beams. Most of the high-LET events registered in the D3 detector exceed the upper energy loss range limit of that detector and were registered in the highest spectral channel as events of 10 MeV.

For the 30° exposure the D3 detector was outside the main beam and for the 60° exposure both D2 and D3 were outside the main beam. That is why only scattered background beams in the low-LET ranges were registered in them.

As a result of the calibrations the Liulin-5 measurement range of LET(H_2O) was estimated to be $0.65\text{--}90 \text{ keV}\mu\text{m}^{-1}$. This makes it possible for Liulin-5 to measure the low-LET components of cosmic radiation as well as a significant part of the biologically relevant high-LET heavy ion component of GCR that contributes to the radiation doses on the ISS.

The Liulin-Phobos flight unit was calibrated with proton and heavy ion beams at the cyclotron and at the HIMAC accelerator at the NIRS, Japan in January–February 2009. The calibrations were performed in agreement with the Memorandum of Understanding on collaboration concerning development, calibration, space flight measurements and data analysis of the Liulin-F instrument onboard the Phobos-Soil mission, which was signed between STII-BAS, IBMP-RAS and NIRS, Chiba, Japan.

As an example of the results obtained, Fig. 8 shows the energy deposition spectrum in the D2 detector in coincidence mode with D1 (LET spectrum) of ^{20}Ne ions with an energy of 600 MeV/n (Semkova et al., 2009). The distribution was obtained at 0° incli-

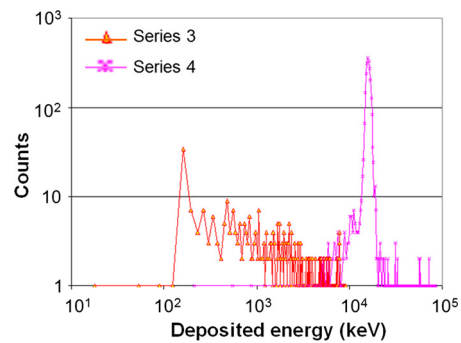


Fig. 8. LET spectrum of ^{20}Ne 600 MeV/u, obtained in the D1&D2 telescope at 0° inclination of the telescope axis to the incident beam.

nation of the telescope's D1–D2 axis to the ion beam. The left part of the LET distribution was measured in the low-LET range of the detector and is mainly due to secondary radiation resulting from interactions of the primary neon beam with surrounding materials. The main peak represents the LET distribution of the neon ions and was measured in the high-LET range of this detector. The obtained LET(H_2O) of ^{20}Ne 600 MeV/n is $26.7 \text{ keV}/\mu\text{m}$ and is in good agreement with the theoretically calculated value of $25.5 \text{ keV}/\mu\text{m}$, keeping in mind the shielding of the detectors. The results of the Liulin-Phobos calibrations at NIRS confirm the correctness of the preliminary electronic calibrations.

3. Main experiments and results in space

3.1. LIULIN experiment on the MIR space station

The Bulgarian–Russian dosimeter–radiometer LIULIN (see Table 1, Item No. 1) was installed in the working compartment of the MIR space station (Dachev et al., 1989). The effective mass thickness of screening matter inside the working compartment of MIR was evaluated to be $6\text{--}15 \text{ g cm}^{-2}$. Thus the main contribution to the count rate is given by protons and electrons that, outside MIR space station, have energies greater than 70 MeV and 10 MeV, respectively. It uses a silicon detector with a thickness of $306 \mu\text{m}$ and an area of 1.8 cm^2 . Simultaneous measurements of the energy absorbed in the detector and of the flux of particles were recorded and transmitted to Earth. The noise level of the detector and electronics was 83 keV. The dose sensitivity was 1 nGy/pulse . The detector unit (see Table 1, Item No. 1) is a miniature, portable, self-indicating device. The LIULIN-microcomputer unit (MCU) is an eight-bit microprocessor unit.

The most significant results obtained by the LIULIN device are:

- During the declining phase of the 22nd solar cycle the GCR fluxes observed on the MIR space station at $L > 4$ have been enhanced from $50\text{--}70 \text{ }\mu\text{Gy d}^{-1}$ in 1989–1990 up to $130\text{--}140 \text{ }\mu\text{Gy d}^{-1}$ in 1993–1994. L is the McIlwain's L -parameter (McIlwain, 1961; Heynderickx et al., 1996). At the same time the GCR flux increased from an average value of $0.58 \text{ cm}^{-2} \text{ s}^{-1}$ in 1991 up to $1.53 \text{ cm}^{-2} \text{ s}^{-1}$ in 1991 (Dachev et al., 1999a).
- The peak value of the dose rate and flux of particles measured by LIULIN in the SAA increased gradually by a factor of 2 between 1991 and 1994 at an altitude of 410 km. The increase is attributed to the decrease of the atmospheric density during the declining phase of solar activity, which is due to the lower rate of heating of the upper atmosphere when the solar ultraviolet (UV) and extreme ultraviolet (EUV) radiation diminishes during solar minimum. A power law relationship has been deduced between the local atmospheric density at the altitude of the MIR station and the maximum dose rate in

the center of the SAA when the neutral density decreased from $8 \times 10^{-15} \text{ g cm}^{-3}$ to $6 \times 10^{-16} \text{ g cm}^{-3}$; the maximum dose increases from 200 to 1200 mGy h^{-1} , while the particles flux increased from 30 to 120 $\text{cm}^{-2} \text{s}^{-1}$ (Dachev et al., 1999a).

- LIULIN measurements represent the low altitude manifestation of radiation belt dynamics. Before the 23–26 March 1991 solar-geomagnetic events LIULIN dose and flux data exhibited a maximum located at $L \sim 1.4$ in the region of the SAA. This is due to the particles from the inner radiation belt. After the March 23 1991 geomagnetic storm a “new” maximum in the LIULIN flux data was created at $1.8 < L < 2.2$. This was a unique phenomenon (http://www.stp.isas.jaxa.jp/akebono/RDM/rdm/rdmflux_1989_2010.gif) not reported before or since. It was a relatively stable configuration observed during the whole of 1991 independent of the geomagnetic conditions. It was identified in the LIULIN data taken through the middle of 1993. The outer radiation belt maximum was frequently observed after geomagnetic disturbances as a dynamic structure for 1–3 months. The ORB in the MIR data was usually located at $2.5 < L < 3.2$. After extended quiet conditions it disappeared (Dachev et al., 1998b).
- Several large SEP took place during the LIULIN observations. SEP data are available for September 29, 1989, October 18, 1989, March 23, 1991, June 8 and 15, 1991 and June 26, 1992. Data analysis of these events is presented in the paper by (Shurshakov et al., 1999).

3.2. Experiments and results on ISS

The largest number of Liulin experiments in space since 2001 have been performed on the ISS, including: Liulin-E094 (April–August 2001), Liulin-ISS (September 2005–June 2014), Liulin-5 (May 2007–present), R3DE (February 2008–September 2009) and R3DR (March 2009–August 2010) (see Table 1, Part 1 Items Nos. 3, 5, 6 and Part 2 Items 9, 11). Two of them, Liulin-ISS and Liulin-5, are still working. The R3DR experiment was repeated as part of the EXPOSE-R2 mission for 1.5 years starting in October 2014 on the Russian Zvezda module of the ISS (http://www.nasa.gov/mission_pages/station/research/experiments/211.html).

3.2.1. DES data selection procedure

The data selection procedure was established for DES instruments to distinguish between the three expected radiation sources: (1) GCR particles, (2) protons with more than 15.8 MeV energy in the SAA region of the IRB and (3) relativistic electrons with energies above 0.78 MeV in the ORB (Dachev, 2009). Fig. 9 confirms these features in the R3DR data. The abscissa plots the measured flux in $\text{cm}^{-2} \text{s}^{-1}$, while the ordinate shows the dose rate in $\mu\text{Gy h}^{-1}$ and the dose rate to flux ratio (D/F) (or specific dose SD) in $\text{nGy cm}^{-2} \text{ particle}^{-1}$ (Dachev, 2009; Heffner, 1971) for the period 1 April–7 May 2010, which is distinguished by very high ORB fluxes and dose rates (Dachev et al., 2012b). The large number of experimental points (295,374 points) in the diagonal of the figure is responsible for the dose rate values, which, as expected, are linearly dependent on the flux, while the points lying almost horizontally represent the D/F ratio.

Three branches in each graphic take the form of a left hand wrist with two fingers. The wrist represents a highly populated part in the diagonal group of points: (1) a large number of the measured points are in the range $0.03\text{--}30 \mu\text{Gy h}^{-1}$ and (2) for a fixed flux a wide range of doses is observed. These two features could be explained only by GCR particles which, being relatively less abundant and having high LET, deposit varying doses for the same flux. The smallest dose rates ($0.03\text{--}0.430 \mu\text{Gy h}^{-1}$) are observed close to the magnetic equator, while the largest ones are observed at high latitudes. In the horizontal graphic this part of

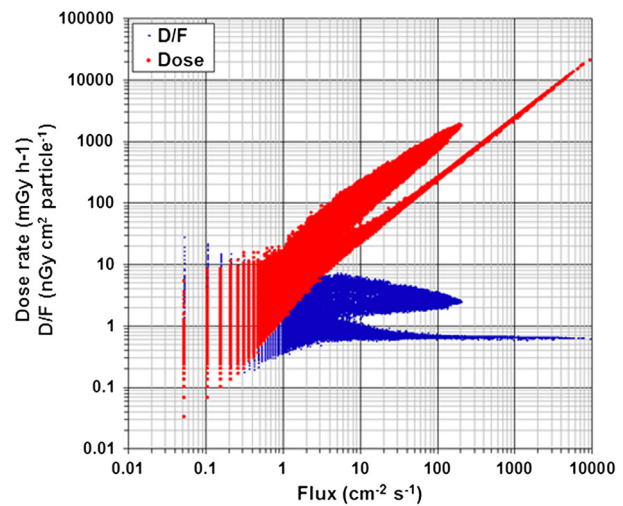


Fig. 9. Characterization of the R3DR predominant radiation sources by the dose rate from flux and dose to flux (D/F) dependencies.

the data is represented with a similarly large number of points, which in large part overlap the dose rate diagonal points.

The “index finger” is in the dose rate range $9\text{--}22,000 \mu\text{Gy h}^{-1}$ and takes the form of a straight line. Its representation in the horizontal graphic is a finger extending up to 10,000 in $\text{cm}^{-2} \text{ s}^{-1}$, with dose to flux values below $1 \text{ nGy cm}^2 \text{ particle}^{-1}$. This finger is based on low LET particles and could be formed only by relativistic electrons (Dachev et al., 2009) in the outer radiation belt.

The “big” finger in the diagonal graphic has a different source than the previous two because it is characterized by a high range of doses for a fixed flux but the dose rates are in the range $30\text{--}1900 \mu\text{Gy h}^{-1}$. This number of points could only represent protons from the IRB (in the region of the SAA) whose dose depositions depend on the energy. The lower energy protons deposit higher doses. In the horizontal graphic this finger has a similar form and is situated in the range $1.2\text{--}8 \text{ nGy cm}^2 \text{ particle}^{-1}$. Both IRB and ORB fingers can be approximated by straight lines. From these approximations we calculate that 1 proton in the IRB deposits on average a dose of 1.4 nGy in the silicon detector, while 1 electron in the ORB deposits a dose of 0.33 nGy , in good agreement with Heffner's formulae (Heffner, 1971).

The conclusion which can be drawn from Fig. 9 is that the data can be simply split in two parts by the requirements for the ratio $D/F < 1$ and $D/F > n\text{Gy cm}^2 \text{ particle}^{-1}$. This will generate graphics that will divide the IRB and ORB sources. GCR protons in equatorial and low latitude regions have very small fluxes of less than $1 \text{ particle cm}^2 \text{ s}^{-1}$, which is why the D/F ratio is not stable and varies in the range from 0.03 to $30 \text{ nGy cm}^2 \text{ particle}^{-1}$ (Dachev et al., 2012b). This variation makes the D/F ratio inapplicable for the characterization of the GCR radiation.

3.2.2. Liulin-E094 results

The first use of the DES in space was in the Liulin-E094 instrument (see Table 1, Part 1, Item No. 3), that was developed, qualified for space and used in the ESA Dosimetric Mapping-E094 experiment (Reitz et al., 2005) on the US Laboratory module of the ISS as a part of the Human Research Facility in May–August, 2001 (Dachev et al., 2002). The main purpose of this experiment was to investigate the dose rate distribution inside the US Laboratory module and Node-1 of ISS.

Dachev et al. (2006) developed a 3-D shielding model of the MDU unit and located it in four locations in the ISS shielding model. Using the trapped proton differential spectra generated from the SPENVIS (<http://www.spenvis.oma.be/>) on-line capability for calculation of AP8 trapped proton spectra and the high-

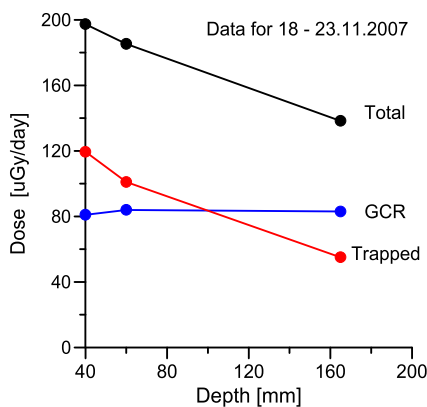


Fig. 10. Typical depth dose distribution along the radius of the phantom. Circles mark the total, GCR and SAA trapped proton doses along the radius at 40, 60 and 165 mm distance from the phantom surface.

energy proton transport code PDOSE we were able to calculate the doses at each MDU location. The differences between the observed Liulin-E094 MDU doses and the calculated ones do not exceed 15%. The obtained data were also used by colleagues from the US for validation of the high-charge and energy (HZE) transport computer (HZETRN) code (Wilson et al., 2007; Nealy et al., 2007; Slaba et al., 2011) and by Badavi (2014) for validation of the new trapped environment AE9/AP9/SPM at LEO.

3.2.3. Liulin-ISS results

The Liulin-ISS instrument (see Table 1, Part 1, Item No. 3) was launched to the Russian segment (RS) of the ISS in September 2005. It contains four MDUs with control and interface units and displays and was used in the Service Radiation Monitoring System of the RS of the ISS (Dachev et al., 1999b). The following information can be displayed: current dose in $\mu\text{Gy h}^{-1}$, current event rate (flux) $\text{cm}^{-2} \text{s}^{-1}$, accumulated dose mGy initiated by the "Switch ON". The battery operation time of the MDU is about 7 days. The 4 MDUs can be used as personal dosimeters in case of an SEP event. Because of some unexpected problems with the telemetry system connections, the instrument was not used as planned and now a new instrument named Liulin-ISS-2 is under development with similar functions, which is expected to be in space in the next 2–3 years.

3.2.4. Liulin-5 results

The Liulin-5 DT instrument (see Table 1, Part 1, Item No. 5) (Semkova et al., 2003) was launched to the RS of the ISS in May 2007. Measurements with Liulin-5 were conducted in the spherical tissue equivalent phantom of the Matroska-R experiment located in the PIRS-1 module of the ISS in the period July 2007–March 2010, corresponding to the minimum of solar activity in the 23rd solar cycle. In addition, measurements corresponding to the maximum of the 24th solar cycle were conducted from December 2011 to April 2014 both inside and outside the phantom located in the MIM1 module of the ISS. The main results obtained during the minimum of the 23rd solar cycle have been published (Semkova et al., 2012, 2013a, 2013b, 2013c).

A typical depth-dose distribution along the radius of the spherical phantom located in the PIRS-1 module of the ISS is shown in Fig. 10. The average daily absorbed doses at 40 mm depth in the phantom (corresponding approximately to the shielding of the blood-forming organs in the human body) are between $180 \mu\text{Gy d}^{-1}$ and $220 \mu\text{Gy d}^{-1}$. At that depth the contribution of the trapped protons is about 50–60% of the total absorbed dose and the rest of the dose is from GCR. At 165 mm distance from the phantom surface the dose decreases by a factor of 1.6–1.8 compared to the dose at 40 mm depth in the phantom. At that distance

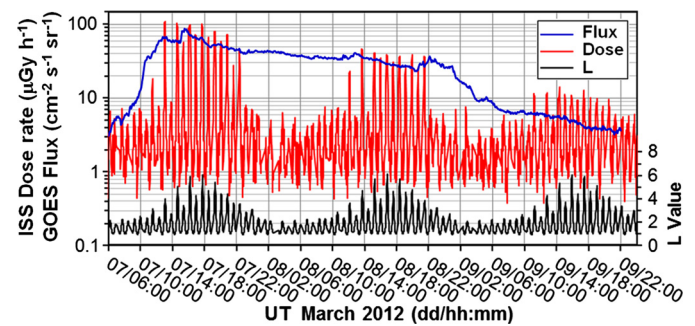


Fig. 11. Flux of protons with energies ≥ 100 MeV measured by GOES-13 (blue curve), the dose rate in D1 detector of Liulin-5 measured outside the SAA (red curve), and the corresponding L-values (black curve) versus time during the March 2012 SEP event. (For interpretation of the references to color in this figure legend, the reader is referred to the web version of this article.)

(near the phantom's center) the GCR contribute about 60% of the total dose.

The average quality factor for different time intervals of 5–7 days is between 2.7 and 4.4; the average dose equivalent rates are $550\text{--}880 \mu\text{Sv d}^{-1}$. The dose equivalent of GCR and their secondary particles represents at least 70% of the total dose equivalent at 40 mm depth with the balance from trapped protons.

During the SEP events of 7–12 March 2012 (see Fig. 11) at $L > 3$ the particle flux and dose rates increased in all three detectors of the Liulin-5 charged particle telescope located at 40, 60 and 165 mm depths along the radius of the tissue-equivalent spherical phantom in MIM1 module of ISS (Semkova et al., 2013c).

The additional absorbed dose at 40 mm depth in the phantom received from the SEP event on 7–9 March 2012 was approximately $180 \mu\text{Gy}$. The additional dose equivalent at 40 mm depth in the phantom received from that event was about $448 \mu\text{Sv}$. The additional exposures received from the SEP event are comparable to the average absorbed daily dose and dose equivalent measured in the spherical phantom in the ISS during quiet periods. In Fig. 11 it can be seen that there is a good agreement of the Liulin-5 dose rates trend during the SEP event with the proton flux of energies ≥ 100 MeV (able to penetrate into the ISS) measured by the GOES-13 satellite (blue line).

3.2.5. R3DE instrument results

The R3DE instrument (see Table 1, Part 2, Item No. 9) with a 256 channel ionizing radiation monitoring spectrometer, a 3 channel UV and a 1 channel photosynthetically active radiation (PAR) spectrometer functioned on the ESA European Technology Exposure Facility (EuTEF) platform inside the EXPOSE-E facility outside of the European Columbus module of the ISS between 20 February 2008 and 1 September 2009 with 10-s resolution behind 0.45 g cm^2 of shielding (Horneck et al., 1998; Dachev et al., 2012a; Schuster et al., 2012).

There are two major discoveries connected with the ionizing radiation monitoring spectrometer of the R3DE instrument. The first is the already mentioned large doses from relativistic electrons (Dachev et al., 2012a, 2012b; Dachev, 2013a); the second is the decrease in the SAA dose rate during the dockings of the US space shuttle with the ISS (Dachev et al., 2011d).

Fig. 12 shows the results of measurements of the SAA doses for the time span 22 March 2008–9 January 2009. SAA proton energies in MeV, maximal dose rates in $\mu\text{Gy h}^{-1}$ and daily dose rates in $\mu\text{Gy d}^{-1}$ are presented in the two panels. The maximal dose rates are the largest values observed during each day. The largest value recorded was $1708 \mu\text{Gy h}^{-1}$ and the average was $1218 \mu\text{Gy h}^{-1}$.

The relatively low dose rates at the left side of Fig. 12 have to do with the ISS altitudes in the range of 350–365 km. The increase

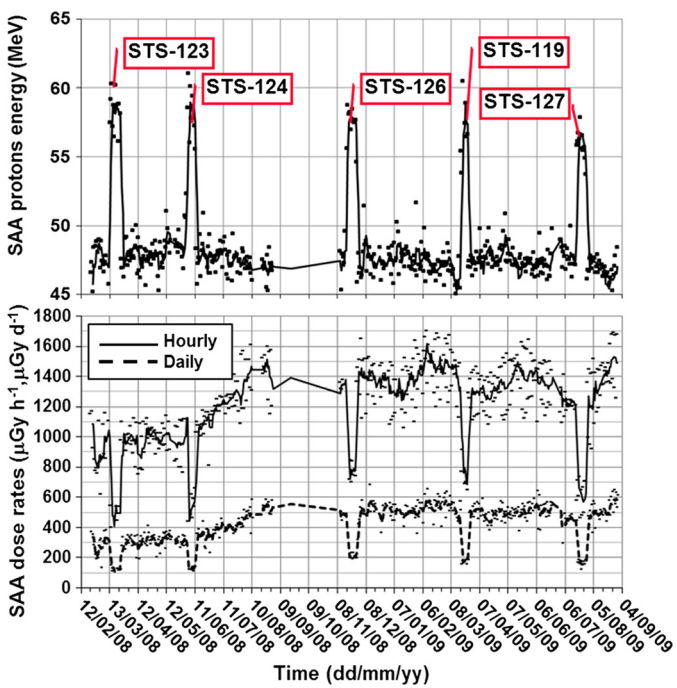


Fig. 12. Daily and hourly SAA dose rates and SAA proton energies measured with the R3DE instrument during the EXPOSE-E mission. The space shuttle dockings at the ISS create strong decreases in the hourly and daily dose rates due to the additional shielding effect of the space shuttle body on the R3DE detector. At the same time the referent energy of the protons in the SAA increases. The space shuttle visits are marked with the STS mission number.

of the station altitude up to 365–375 km after 21 June 2008 led to an increase of the maximal SAA dose rate above $1200 \mu\text{Gy h}^{-1}$.

The main feature seen in Fig. 12 is that during the five space shuttle docking times the SAA maximal doses fell by $600 \mu\text{Gy h}^{-1}$ and reached an average level of $400\text{--}500 \mu\text{Gy h}^{-1}$ for the STS-123 and STS-124 missions. For STS-126, STS-119, and STS-127, the drop was also $600 \mu\text{Gy h}^{-1}$ from an average level of $1400 \mu\text{Gy h}^{-1}$.

The analysis of the daily average SAA dose rate for the studied period shows that before 21 June 2008 it was around $300 \mu\text{Gy d}^{-1}$, after 21 June 2008 it started to increase and on 31 July it reached a value of $500 \mu\text{Gy d}^{-1}$, the level at which the daily average SAA dose rate stayed until the end of the observations in September 2009. The dockings of the space shuttles decreased the daily average SAA dose rate by about $200 \mu\text{Gy d}^{-1}$. Similar reductions of the SAA dose rates were observed by Semones (2008) with the TEPC in the Columbus module for the period 4–24 March 2008. Because of the larger shielding inside the Columbus module the reduction reported was from 120 to $97 \mu\text{Gy d}^{-1}$ during the STS-123 docking time. Benghin et al. (2008) also reported changes in the ratio of daily dose rates of the unshielded detector numbers 2 and 3 of the DB-8 system during the shuttle dockings.

The dose rate variations caused by the Shuttle dockings are connected with the incident proton energy spectral variations. The energy spectra variation can be understood through variations in the deposited energy spectra. The role of particles with higher energy deposition is decreased, which indicates an increased contribution from higher energy protons. To quantify this effect we introduce the “referent energy”, defined as the proton energy producing energy deposition in the detector equal to the average measured energy deposition. The energy of the protons normally incident to the detector is calculated by using the experimental formula described by Heffner (1971). The investigation of the referent energy of the protons in the SAA region is shown in the upper panel of Fig. 12, which reveals that the shuttle dockings increased this energy from about 48 MeV to 58 MeV. The increase of the referent

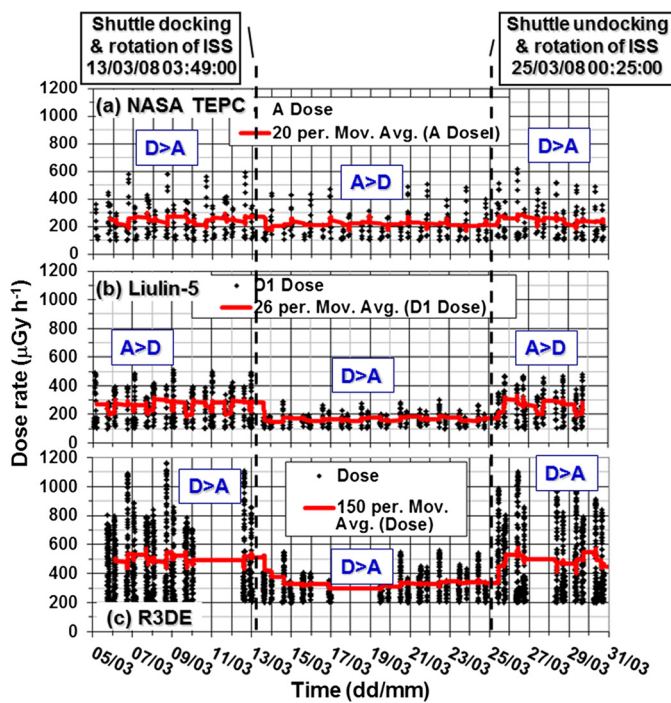


Fig. 13. Variations of the dose rates by the NASA TEPC, R3DE and Liulin-5 instruments close to STS-123 docking in the period 5–31 March 2008.

energy of protons in the SAA region during the shuttle dockings can be explained by the increase of the values in the entire energy range caused by the stopping of the lowest energy protons in the mass of the space shuttle.

Fig. 13 shows the dose rate dynamics observed by 3 different instruments around the time of the Space Shuttle (STS-123) docking and undocking in the time frame 5–31 March 2008. The measured absorbed doses in each exposure interval are represented by black diamonds, while the obtained statistically moving average doses are shown with heavy red lines. The numbers correspond to the number of single measurements used in the moving average calculation.

The three panels contain data as follows: Fig. 13a shows the NASA TEPC absorbed dose rate data, with the selection criterion $>100 \mu\text{Gy h}^{-1}$, representing only the SAA maxima. The first part of the data between 5 March and 14:03:37 on 10 March is from position SM-410, while the second part, through 31 March, is from position COL1A3. Data were obtained from the <http://cdaweb.gsfc.nasa.gov/> server and prepared by N. Zapp; Fig. 13b contains Liulin-5 (Semkova et al., 2007) dose rate data from the first detector, selected in the same way as the TEPC data; Fig. 13c contains R3DE dose rate data selected in the same way as the other two data sets, but with a minimum dose rate of $200 \mu\text{Gy h}^{-1}$.

Because of the large time interval on the x-axis in Fig. 13 the six to eight ascending and descending crossings of the SAA anomaly per day are presented by a pair of bars. The first one corresponds to the descending orbits, while the second one to the ascending orbits during one series of 6–8 crossings. The differences in the dose rate amplitudes are produced by the east–west asymmetries of the proton fluxes in the region of the SAA (Wilson et al., 2007). These amplitudes are additionally affected by changes in the attitude of the ISS, which changes by 180° during the Shuttle docking period and is reversed afterward (Chernykh et al., 2008).

The relations between ascending and descending amplitudes of the dose rates for each instrument before, during and after the Shuttle docking are denoted by text boxes, which contain inequalities labeled by $D > A$ when the descending dose rates were greater than the ascending ones and in reverse with $A > D$ when the

other relation was fulfilled. For the R3DE instrument there were no changes of the amplitude relations. At all times the descending dose rate value was greater than the ascending one. This behavior can be explained by the position of the R3DE instrument on the top of EuTEF where it is not shadowed by the Columbus body from SAA protons drifting to the west. The other two instruments showed rotation of the ascending/descending inequalities connected with the Shuttle docking. These relations are explained more precisely in the next paragraph.

It is clear that all three data sets recorded a decrease in the dose rates after the docking of the Space Shuttle at 03:49 on 13th of March 2008. To emphasize the decreases moving averages lines are calculated and presented by heavy lines in each panel of Fig. 13. For the R3DE the decrease in the moving averages was from 500 to 300 $\mu\text{Gy h}^{-1}$ or about 40% from the value before the docking. The Liulin-5 data decreased from 300 to 180 $\mu\text{Gy h}^{-1}$ or again about 40% from the value before the docking. The TEPC dose rates show the smallest decrease of from 280 to about 200 $\mu\text{Gy h}^{-1}$, which is an approximately 30% decrease. After the space shuttle undocked at 00:25 on 25 March dose rates measured by all three instruments returned to their pre-docking levels.

3.2.6. R3DR instrument results

The R3DR spectrometer (see Table 1, Part 2, Item No. 11) was launched inside of the EXPOSE-R facility to the ISS in December 2008 and was mounted at the outside platform of the Russian Zvezda module of the ISS. The first data were received on March 11, 2009 and the instrument worked almost continuously until the end of August 2010 with 10-s resolution. Comprehensive presentation of the R3DR results inside of the EXPOSE-R facility can be found in Dachev et al. (2015a).

As noted previously, one of the discoveries with the R3DE instrument on the ISS was the large doses from relativistic electrons. Because of less surrounding shielding the relativistic electron doses from the R3DR spectrometer are even higher.

Fig. 14 accumulates in the bottom panel all available R3DR data of averaged daily fluences of relativistic electrons (ISS Flu) and daily absorbed dose rates (ISS AD). The daily R3DR absorbed dose rates closely follow the daily fluence, with a strong linear dependence between them, as expected from Eq. (1). The R3DR daily fluences were obtained from the available flux data specifically for comparison with the GOES-11 daily fluence data for energies above 2 MeV. (See MA GOES curve in Fig. 14.) This comparison is possible because on average location the ISS ORB fluence data were taken at $L = 4.4$, whereas the GOES-11 daily fluence data were obtained at $L = 6.6$. The daily global Ap index (Ap index is averaged planetary daily index), which characterize the geomagnetic field activity (<http://www.swpc.noaa.gov/products/planetary-k-index>) is shown in the upper panel of Fig. 14. All curves represent the moving average (MA) over 2 points of the raw data.

As seen from the upper panel in Fig. 14 the period between 1 March 2009 and 1 March 2010 was characterized by low solar and magnetic activity, which is the main reason for the low ORB activity. Despite the small Ap indexes in this period, Fig. 6 shows that each increase in the Ap or each new magnetic storm increased the fluence recorded on both satellites, GOES and ISS (Zheng et al., 2006).

The most interesting period in Fig. 14 began on 1 April 2010 and covered all data through 20 August. The R3DR and GOES-11 daily relativistic electron fluences increased almost explosively on 6 and 7 April. Although the magnetic storm on 6 April was moderate (daily $Ap = 49$, minimal $Dst = -72 \text{nT}$ at about noon), the second largest fluences in the history of GOES of electrons with energies greater than 2 MeV were recorded. The in the GOES-11 fluence of electrons with energies greater than 2 MeV increased

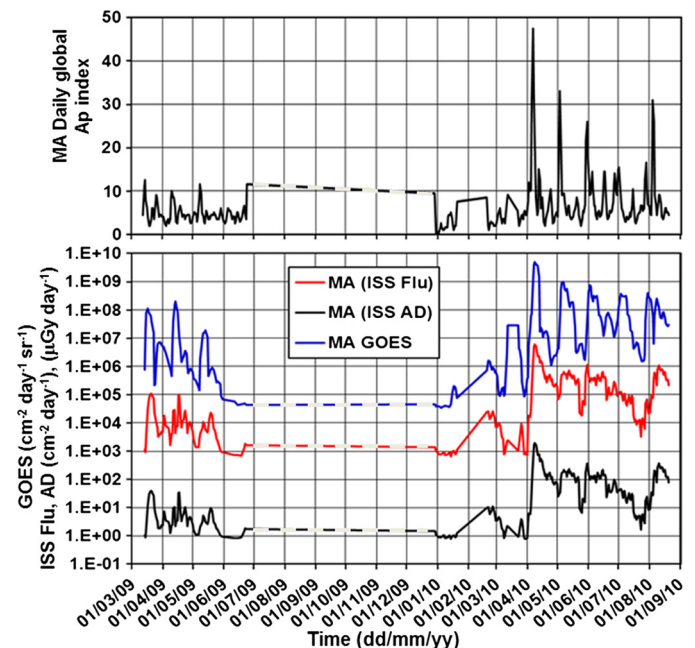


Fig. 14. Results for the daily ORB dose rate (ISS AD) deposited by electron fluence (ISS flu) measured with the R3DR instrument on ISS. These data are compared with the daily GOES-11 satellite >2 MeV (GOES) fluence and the daily global Ap index in the upper panel. (All curves in the lower panel represent the moving average (MA) over 2 points of the raw data.)

by 4.5 orders of magnitude, whereas the R3DR $> 1.18 \text{ MeV}$ daily fluences and daily absorbed doses increased less than 3.5 orders of magnitude. Up until the end of the measurements with the R3DR instrument on 20 August 2010, a few smaller Ap maxima were observed and they were reflected in very similar responses on the GOES satellite, while the correlation with ISS data was much weaker. The geomagnetic conditions on 2–3 May 2010 were similar in magnitude as those on 6 April, but the response of the R3DR daily fluence and dose rate of the 3 May storm was about 1.5 orders of magnitude less than the 5–6 April response. We do not have any explanation for these large differences in the responses and we hope that our experimental data will support the theoretical study of the ORB physics.

In the case of very high daily relativistic electron fluxes as on 7 April 2010 the daily absorbed ORB dose rate increased up to $2348 \mu\text{Gy d}^{-1}$, which is much higher than that of the IRB and GCR sources. During this period of intense ORB energetic electrons precipitations, three EVAs were performed by the STS-131 astronauts on 9, 11 and 13 April 2010 (http://www.nasa.gov/mission_pages/shuttle/shuttlemissions/sts131/main/index.html). The accumulated doses (mainly from ORB and GCR) calculated from R3DR measurements during those 6 h EVAs were between 440 and 300 μGy . These values pose no extreme danger to the health of the astronauts because the daily average absorbed dose rates inside of the ISS, reported by Reitz et al. (2005), vary in the range $74\text{--}215 \mu\text{Gy d}^{-1}$. The relativistic electrons did not have enough energy to penetrate into the body of the astronauts and therefore deposited their dose mainly in the skin and eyes.

In Fig. 4 there is a comparison of data obtained simultaneously by the R3DE/R instruments and the NASA TEPC. The main conclusion from the comparisons of data between the R3DE and R3DR instruments (Dachev, 2013a) is that the values of the dose rates produced by different radiation sources around the ISS exhibited large and rapid variations in space and time. All of these data can be interpreted as possible doses obtained by cosmonauts and astronauts during EVA because the R3DE/R instrument shielding is very similar to the average shielding in both Russian and Ameri-

can EVA suits ([Benton et al., 2006](#)). Fast, real-time measurements at the body of each astronaut to obtain the exact dynamics of the dose accumulation during EVA are required.

An instrumental solution was proposed in [Dachev et al. \(2011e\)](#), where the possible hardware and software improvements for a new Liulin type dosimeter were outlined. New instruments will be able, on the basis of the analysis of the shape of the deposited energy spectrum and the value of the dose to flux ratio, to distinguish among the different types of radiation sources in the ISS radiation environment: GCR, IRB protons and outer radiation belt electrons. They will measure, calculate, store and display the fast variations of the absorbed and ambient dose equivalent doses in any of the possible surrounding mass distributions.

3.3. Experiments and results on satellites

3.3.1. Results obtained by Foton M2/M3 satellites

The Radiation Risks Radiometer-Dosimeter (R3D) for Biopan (R3D-B) with a 256 channel ionizing radiation monitoring spectrometer, a 3 channel UV and a 1 channel PAR spectrometer known as R3D-B2 (see [Table 1](#), Part 1, Item No. 3) was successfully flown 31 May–16 June 2005 inside the ESA Biopan-5 facility on the Foton M2 satellite. The operation time of the instrument was about 20 days for filling the 1.0 MB flash memory with 30-s resolution ([Häder et al., 2009](#)). The R3D-B3 spectrometer (see [Table 1](#), Part 1, Item No. 7) had almost the same mechanical characteristics as those of the R3D-B2, but a larger 2.0 MB flash memory was used for about 30 days' worth of measurements. It was successfully flown 14–29 September 2007 inside the ESA Biopan-6 facility on the Foton M3 satellite. Together with the R3D-B3, the Liulin-Photo instrument (see [Table 1](#), Part 2, Item No. 8) was flown inside the capsule of the Foton M3 satellite ([Damasso et al., 2009](#)). The most important findings in the R3D-B2/B3 data were the measurements of high doses delivered by relativistic electrons at altitudes below 300 km and latitudes above 50° geographic latitude in both hemispheres ([Dachev et al., 2009](#)).

3.3.2. Results obtained at Chandrayaan satellite

The RADOM spectrometer-dosimeter (see [Table 1](#), Part 2, Item No. 10) was successfully used on the Indian Chandrayaan-1 Moon satellite from 22 October 2008–30 August 2009. It started working 2 h after the launch with 10-s resolution behind about 0.45 g cm⁻² shielding. The instrument sent data for a number of crossings of the Earth's radiation belts and continued to function on 100 and 200 km circular lunar orbits, mainly measuring the GCR environment ([Dachev et al., 2011c](#)).

Chandrayaan-1 was placed into a lunar transfer trajectory on 3rd November 2008 (13 days after launch) and a lunar orbit capture manoeuvre was carried out on 8th November (18 days after launch). [Fig. 15](#) shows RADOM observations for about 3 days before the lunar orbit capture and about one day after it. More than 40 000 measurements with 10-s resolution were used for the figure. [Figs. 15b and 15c](#) show the moving average over 200 points of measured particle flux and the absorbed dose rate, respectively. [Fig. 15d](#) shows the distance from the Moon (in km), while [Fig. 15a](#), shows the Oulu Neutron Monitor running average of measured count rate per minute averaged over 10 min. The average dose rate from more than 33,000 measurements in the altitude range between 308,000 and 20,000 km from the Moon is ~12.76 µGy h⁻¹. The range of the real measured dose rates is between 3.34 and 41.34 µGy h⁻¹ with a standard deviation of 4.25 µGy h⁻¹. The average flux is 3.14 particles cm⁻² s⁻¹, while the real flux range is between 1.71 and 4.82 particles cm⁻² s⁻¹ with a standard deviation of 0.41 cm⁻² s⁻¹. [Figs. 14b and 14c](#) do not show this real dynamics of the values because the moving averages are plotted

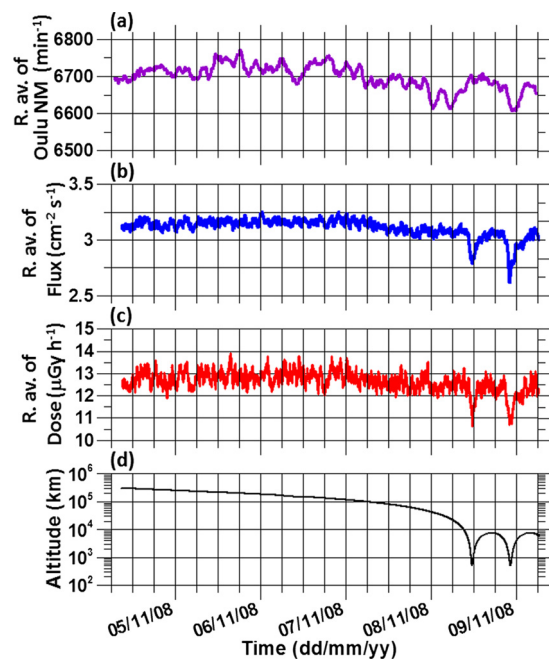


Fig. 15. RADOM observations during lunar transfer trajectory and lunar orbit capture. The distance is from the Moon. The trends in particle flux coincide with the Oulu neutron monitor data trends.

there. These values of the dose rate and flux may be used as reference values for the deep space radiation conditions at this very low level of solar activity.

For the above mentioned altitude range the flux correlates with the Oulu NM count rate and with the solar activity, respectively. Later on during the two closer approaches to the Moon at an altitude about 508 km the flux and the dose rate decreased due to the enhanced shielding of the cosmic rays by the Moon itself. A closer look at [Fig. 15b](#) reveals that the second periselene crossing is deeper than the first one. This is largely related to a local increase of the solar activity as evident from the simultaneous decrease of the Oulu NM count rate.

RADOM observations which began within two hours after launch of the Chandrayaan-1 and continued until the end of the mission demonstrated that it could successfully characterize different radiation fields in the Earth and Moon environments. Signatures and intensities of proton and electron radiation belts, relativistic electrons in the Earth magnetosphere as well as GCR were clearly identified and measured. The effect of the solar modulation of GCR could also be discerned in the data. The electron radiation belt doses reached ~40,000 µGy h⁻¹, while the maximum flux recorded was ~15,000 cm⁻² s⁻¹. The proton radiation belt doses reached their highest values of ~130,000 µGy h⁻¹, while the maximum flux was ~9600 particle cm⁻² s⁻¹. Comparison of these results with other similar instruments on board the ISS shows good consistency, indicating nominal performance of RADOM. Outside the radiation belts, en-route to the Moon, the particle flux (~3 particle cm⁻² s⁻¹) and corresponding dose were very small (~12 µGy h⁻¹) which further decreased slightly in the lunar orbit because of the shielding effect of the Moon. Average flux in lunar orbit was ~2.45 cm⁻² s⁻¹ and the corresponding absorbed dose rate was 9.46 µGy h⁻¹ at 100 km orbit. These increased to 2.73 particles cm⁻² s⁻¹ and 10.7 µGy h⁻¹, respectively, at the 200 km orbit. These results were recently compared by [Reitz et al. \(2012\)](#) to theoretical calculations using Monte-Carlo simulations and good agreement was obtained. The total accumulated dose during the transfer from Earth to Moon was found to be ~1.3 Gy.

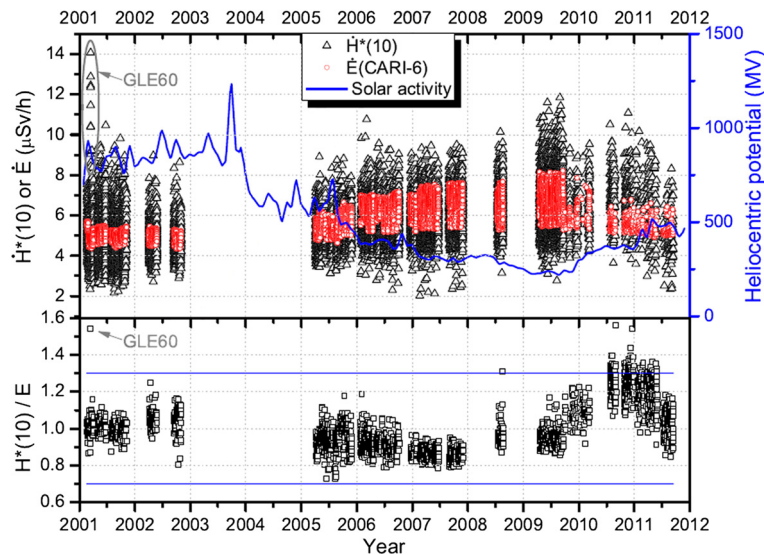


Fig. 16. Top graph: $H^*(10)$ rates determined by Liulin and E rates calculated with CARI-6 code (Friedberg et al., 1992) plotted as a function of time (only data from FL350 (10.67 km) and effective vertical cut-off rigidity (VCR) ≤ 3.5 GV are shown). Solar activity is expressed via the heliocentric potential (O'Brien et al., 2005). Bottom graph: Ratios of integral values per whole flight between ambient dose equivalents, $H^*(10)$, estimated with Liulin, and effective doses, E , calculated with CARI-6 plotted as a function of time. $\pm 30\%$ confidence band is plotted.

An instrument similar to the RADOM is under development for the future Russian Luna-Glob mission (Dachev et al., 2013a).

3.3.3. Results obtained at "BION-M" No. 1 and "Foton-M" No. 4 spacecraft

"BION-M" No. 1 was a low Earth orbit satellite that orbited the Earth with a period of 89.9 min, near the Earth's equator and at an altitude above the Earth's surface in the range 253–585 km. The final orbit of the satellite was almost circular with an apogee of 585 km and a perigee of 555 km altitude. The final orbital parameters were reached after 21 April 2013 (Dachev et al., 2015b). Space radiation has been monitored using the RD3-B3 spectrometer-dosimeter (see Table 1, Part 2, Item No. 13), which was mounted inside of the satellite in a pressurized volume together with biological objects and samples. The RD3-B3 instrument is a battery-operated version of the spare model of the R3D-B3 instrument developed and built for the ESA BIOPAN-6 facility on the Foton M3 satellite in September 2007 (Damasso et al., 2009).

The observed maximal hourly ($4530 \mu\text{Gy h}^{-1}$) and average daily ($908 \mu\text{Gy d}^{-1}$) IRB dose rates values at the "BION-M" No. 1 satellite are the highest observed by us because the altitude of the "BION-M" No. 1 orbit was the highest in comparison with other DES satellite measurements in LEO. The same is true for the average daily GCR doses, which reached $102.8 \mu\text{Gy d}^{-1}$. The observed ORB doses are smaller than the ones measured outside the ISS because of the higher shielding on the "BION-M" No. 1 satellite.

An experiment very similar to the "BION-M" No. 1 experiment was performed between 18 July and 1 September 2014 on the Foton-M" No. 4 spacecraft using the same RD3-B3 spectrometer-dosimeter (see Table 1, Part 2, Item No. 14). The satellite was placed in an elliptical orbit (573–260 km) with inclination 65° . The apogee of the orbit slowly decreased to 542 km which is why the IRB dose rates decrease from 540 to $340 \mu\text{Gy d}^{-1}$. The daily GCR doses were stable with an average value of $100.6 \mu\text{Gy d}^{-1}$.

3.4. Major experiments and results on aircraft, balloons and rockets

Table 2 lists DES Liulin type experiments on aircraft, balloon, rocket and mountain peaks. The pictures shown for items 2 and 8 are the latest versions of the instruments used in this category.

(Some of the instruments had housings different from those pictured.)

The Liulin-4C, MDU#2 instrument (see Table 2, Item No. 1) worked successfully during the flight of a French balloon up to 32 km altitude in the region of the Gap town in southern France on 14th of June 2000. This experiment was performed by Prof. Frantisek Spurny from the Nuclear Physics Institute, Czech Academy of Sciences (Spurny, 2000).

One battery-powered DES of Liulin-4J (see Table 2, Item No. 1) type performed dosimetric measurements of the ionizing radiation environment at ~ 20 km altitude aboard NASA's Lockheed ER-2 high altitude research aircraft in October–November 2000 from Edwards Air Force Base (AFB) in Southern California on flights over the border region dividing Central California from Central Nevada (Uchihori et al., 2003c).

The Mobile Dosimetry Units MDU-5 and 6 (see Table 2, Item No. 2) were used for long-term measurements between 2001 and 2014 on Czech Airlines (CSA) aircraft on different routes. Data obtained were used for comparison with model calculated doses for the purpose of individual monitoring of aircraft crews (Ploc, 2009; Spurny et al., 2009; Ploc et al., 2011). Fig. 16 presents almost one complete solar cycle of data obtained by colleagues from Nuclear Science Institute, Prague, Czech Republic. These data are publicly available at (<http://hroch.ujf.cas.cz/~aircraft/>) in a database of measurements (Ploc et al., 2013). Additional details are in Fig. 16 caption.

Very similar instruments to the Mobile Dosimetry Units MDU-5 and 6 were used by scientific groups in Spain (Sáez Vergara and Dominguez-Mompell, 2009) and Korea (Hwang et al., 2010) for radiation measurements on aircraft.

Three battery-powered DES (see Table 2, Item No. 3) were operated during the 8 June 2005 certification flight of the NASA Deep Space Test Bed (DSTB) balloon at Ft. Sumner, New Mexico, USA. The duration of the flight was about 10 h (Benton, 2005a and 2005b).

Liulin-6S, Liulin-M, Liulin-6MB and Liulin-6R (see Table 2, Item No. 4) are web-based instruments (Matviichuk et al., 2008). They use a web module to generate a web page. The deposited energy spectra data are transmitted via LAN interface by HTTP and FTP protocols. Instruments of this type have functioned for varying periods since 2005 on Jungfrau (Switzerland) at 3453 meters Above

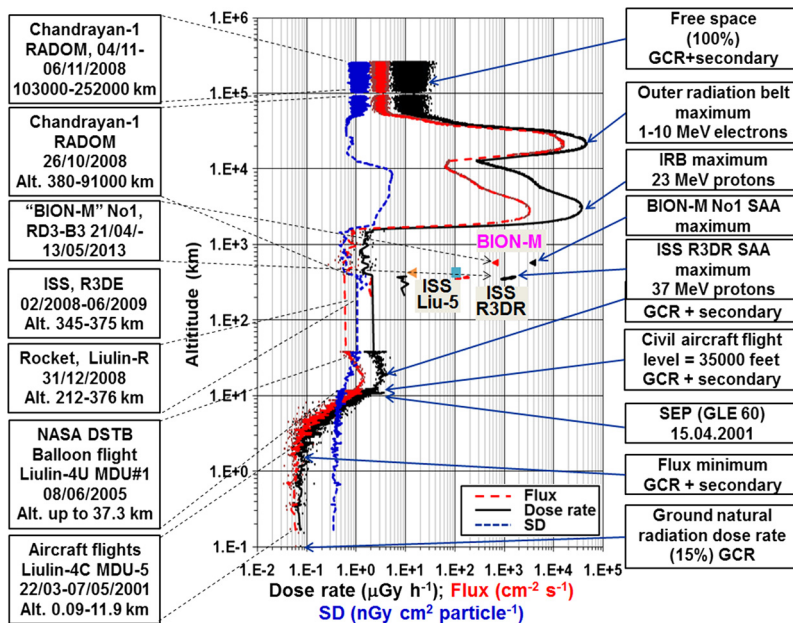


Fig. 17. Variations of the absorbed dose rate, flux and specific dose for altitude range from 0.1 to 250,000 km. (For interpretation of the references to the colors in this figure legend, the reader is referred to the web version of this paper.)

Mean Sea Level (AMSL) (<http://130.92.231.184/>), Moussala (Bulgaria) at 2925 meters AMSL (<http://beo-db.innr.bas.bg/moussala/>) and Lomnický Stit (Slovakia) at 2633 meters AMSL peaks and at the ALOMAR observatory in Norway. The two mountain peak instruments worked well until June 2014 and their data can be accessed online at the URLs in the text above.

The Liulin-4SA (see Table 2, Item No. 5) spectrometer was designed in 2005 at the request of Captain Ian Getley, pilot of Qantas Airways Boeing 747-400 aircraft (Getley et al., 2010). The Liulin-4SA was used inside of the cockpit of the aircraft and provided LCD display data for the local dose rate and flux simultaneously with the flight altitude, longitude and latitude, obtained from the build-in GPS receiver for each measurement interval (usually 60 s). Pre-programmed alert signals could be initiated when the measured dose rate exceed preliminary set levels for more than 3 subsequent measurement intervals.

The two Liulin DES systems presented in Table 2, Item No. 6 consist of 4 dosimetry units (DU) and 1 control and interface unit (CIU). The Liulin-6U instrument was delivered to NASA-Marshall Space Flight Center, USA in 2005. It was planned to be used in a balloon experiment (Adams et al., 2007). The second one was delivered to the Skobeltsyn Institute of Nuclear Physics at Lomonosov Moscow State University in 2010. It was planned to be used in the RAZREZ system for the RADIOSCAF experiment on the ISS (Grigoriev et al., 2010; Petrov et al., 2010).

The Liulin-R instrument (see Table 2, Item No. 7) was successfully launched on a HotPay2 rocket from the Andoya Rocket Range (ARR), Norway, on 31 January 2008 at 19:14:00 UT as a part of an EU-financed scientific program called eARI (ALOMAR eARI project) (Tomov et al., 2008) and attained an altitude of 380 km.

Wissmann et al. (2013) performed five balloon experiments up to 30 km altitude using Liulin-6RG spectrometers (see Table 2, Item No. 8) between July 2011 and August 2012. The Liulin instruments were powered and transmitted the 30 s duration deposited energy spectrum to a data logger developed in Physikalisch-Technische Bundesanstalt (PTB), Germany.

The Liulin spectrometer presented in Table 2, Item No. 9 is the latest generation of a series of instruments with a built-in GPS receiver and a 1 or 2 MB SD card. This type of instrument (LIULIN-4N) was first used by colleagues from the Department of Chem-

istry and Chemical Engineering, Royal Military College of Canada in 2003–2005 (Kitching, 2004; Green et al., 2005). The Canadian group developed two different methods of determining the $H^*(10)$ values from the LIULIN data, and these agree very well the $H^*(10)$ values measured by the TEPC, within the 20% error inherent within both instruments.

4. Conclusions

Many versions of Liulin-type spectrometers have been developed, built and flown on spacecraft, aircraft, balloons, and rockets, as well as used on the ground, between 1988 and 2014.

The main advantages of the Liulin type spectrometers are their low weight (100–500 g), low power consumption (100–500 mW) and low cost.

Confidence in the data obtained is increased by the extensive calibrations of the Liulin devices using a number of different radioactive sources and accelerators.

The data analysis procedure was developed using the calibrations and the great deal of experimental data, and the dose to flux ratio or the specific dose (SD) has been selected and used for characterization of the absorbed and equivalent doses from different radiation sources and the incident energy of the protons incident on the detectors.

One of the main achievements is the use of experimental data from different Liulin instruments flown on aircraft, balloon and satellites to generate a profile of the ionizing radiation exposure between the Earth's surface and free space.

Fig. 17 presents the synthesized altitudinal profiles of the moving averages (over 4 points) of three parameters: absorbed dose rate in $\mu\text{Gy h}^{-1}$ (heavy solid line), flux in $\text{cm}^{-2} \text{s}^{-1}$ (long red dashed line) and specific dose (SD) in $\text{nGy cm}^2 \text{particle}^{-1}$ (short blue dashed line). On the left side of the figure are listed the carriers, instruments, time, averaged geographic coordinates of the measured values and their altitude range in km. On the right side are listed the conditions and predominant radiation sources for the places indicated with the arrows. Fig. 17 is similar to the one published as Fig. 2 in Dachev (2013b) but improved with the new data obtained with the RD3-R3 instrument on the BION-M No. 1 satellite and Liulin-5 data on the ISS for the flight period of the

BION-M No. 1 satellite, 21 April–13 May 2013. Table 1 in Dachev (2013b) gives detailed descriptions of the different points of interest in Fig. 17 and how the data were obtained.

The use of the dose-to-flux ratio or the specific dose (SD) for characterization of the predominant radiation is demonstrated well by the behavior of the SD curve in Fig. 17.

The SD values seen in Fig. 17 are low at the ground with values of 0.3–0.5 nGy cm² particle⁻¹. In the altitude range 1–8 km the SD slowly increase. Further the SD increase to values of about 0.9–1.1 nGy cm² particle⁻¹ at an altitude of 37 km. We interpret this behavior of the SD profile to be due to the change of the radiation field components from predominantly light particles such as electrons, pions and muons at altitudes up to 8 km to heavier particles such as protons and neutrons at altitudes up to 37 km (Bagshaw and Cucinotta, 2007). This hypothesis is confirmed by the increase of the SD values up to 0.7 nGy cm² particle⁻¹ in the maximum of the SEP on 15 April 2001, while the average value for aircraft at 10.67 km is 0.49 nGy cm² particle⁻¹.

The averaged SD values observed with the R3DE instrument on the ISS inside of the SAA maximum was almost equal for ascending and descending nodes. The observed values of 2.33–2.37 nGy cm² particle⁻¹ correspond to protons with energies 37–38 MeV (Heffner, 1971; Dachev, 2009). Similar values of SD were observed with the RADOM instrument at the bottom of the IRB. (See Fig. 17.) Furthermore, with increasing altitude the SD values increased to about 4.6 nGy cm² particle⁻¹ at 9000 km altitudes which corresponds to energies of about 15 MeV (Heffner, 1971; Dachev, 2009). The IRB and Pfotzer maximums are observed at lower altitudes in the flux values as compared to the dose rates. The transformation of the SD values to proton energy values gives 26 MeV in the flux and 24 MeV in the dose rate maximum.

In general the proton energy decreased with altitude across the IRB maximum. The crossings of the slot region led to a dramatic decrease of the SD values below 1 and down to about 0.6–0.8 nGy cm² particle⁻¹, which indicates a change of the predominant radiation source from protons to electrons, as expected when the satellite reached the outer radiation belt. The SD values are larger than the ones predicted by Heffner's formulae due to the additional flux of GCR particles in the ORB. It is remarkable that around the ORB maximum the flux maximum occurred at a lower altitude (20,300 km) while the dose rate maximum was observed at 21,260 km altitude.

Finally, when the satellite reached free space at 230,000 km altitude the averaged SD value recorded was 1.13 nGy cm² particle⁻¹, corresponding to GCR protons with an energy of 169 MeV (Heffner, 1971; Dachev, 2009).

The dose rate and flux data in Fig. 17 cover seven orders of magnitude and can be used for educational purposes and also as reference values for new models. The presentation of data in kilometers above the Earth surface instead of *L* values allows space agencies' medical staffs, who are typically not experts in geophysics, to use them for a first approximation to the expected human exposure at different altitudes and to educate the general public and students about the positions of the most common maxima of exposure in LEO and in free space.

Acknowledgements

We devote this work to the memory of Prof. F. Spurny, Dr. V.M. Petrov and Dr. I.V. Chernykh for their invaluable contribution to the Liulin instrument developments and data analysis. The authors would like to thank: Dr. J. Miller, Lawrence Berkeley National Laboratory, Berkeley, USA for the post-calibrations of LIULIN instrument (Dachev et al., 1998a); Dr. E.G. Stassinopoulos, former Director of NASA-GSFC Radiation Physics Office for the support and help in the LIULIN-3M calibrations (Dachev et al., 2003); Dr. R. Beaujean, for-

mer scientist in Christian-Albrechts-Universitaet zu Kiel, Germany for the cooperation and financial support in the development of the Liulin-4 instrument (Dachev et al., 2002); Prof. J. Lemaire, from Institut d'Aeronomie Spatiale de Belgique for the help in the interpretation of LIULIN data and for the financial support in the development of the Liulin-ISS instrument; Prof. Gh. Gregoire and H. Schmitz from Institut de Physique, Universite Catholique de Louvain, Belgique, for the Liulin-ISS calibrations (Dachev et al., 2002); Prof. E.R. Benton from the Department of Physics, Oklahoma State University, USA for support and NASA balloon data (Benton, 2005a, 2005b); ISRO staff and more specially to: M. Annadurai, Project Director and Prof. J.N. Goswami, Project scientist of Chandrayaan-1 satellite, P. Sreekumar and V. Sharang, Space Astronomy & Instrument Division, ISRO, Bangalore, India for RADOM instrument support (Dachev et al., 2011c); M.T. Giardi and M. Damasso, Institute of Crystallography-National Research Council, Roma, Italy for the Liulin-Photo cooperation (Damasso et al., 2009) as well as other co-authors and organizations listed in the text and in the references for their contribution in the use and data interpretation of the Liulin-type instruments. Many thanks to the cosmonauts and astronauts onboard the Mir space station and the ISS for conducting the experiments with Liulin instruments.

Lastly we acknowledge with thanks the LSSR referees and editors for their comments and suggestions during editing of the paper.

References

- Adams, J.H., Adcock, L., Apple, J., Christl, M., Cleveland, W., Cox, M., Dietz, K., Ferguson, C., Fountain, W., Ghita, B., Kuznetsov, E., Milton, M., Myers, J., O'Brien, S., Seaquist, J., Smith, E.A., Smith, G., Warden, L., Watts, J., 2007. Nucl. Instrum. Methods Phys. Res., Sect. A, Accel. Spectrom. Detect. Assoc. Equip. 579, 522–525.
- Akatov, Yu.A., Eremenko, V.G., Kartsev, I.S., et al., 2002. Spherical phantom for studying radiation conditions in outer space. Nucl. Meas. Inf. Technol. 3, 67–71.
- Badavi, F.F., 2014. Validation of the new trapped environment AE9/AP9/SPM at low Earth orbit. Adv. Space Res. 54, 917–928. <http://dx.doi.org/10.1016/j.asr.2014.05.010>.
- Bagshaw, M., Cucinotta, F.A., 2007. Fundamentals of aerospace medicine cosmic radiation. Available online at: http://ntrs.nasa.gov/archive/nasa/casi.ntrs.nasa.gov/20070028831_2007025868.pdf.
- Bazilevskaya, G.A., Stozhkov, Y.I., Svirzhevskaya, A.K., Svirzhevsky, N.S., 2013. Cosmic rays and radioactivity in the near-ground level of the atmosphere. J. Phys. 409, 012213. <http://dx.doi.org/10.1088/1742-6596/409/1/012213>.
- Benghin, V.V., Petrov, V.M., Drobyshev, S.G., Panasyuk, M.I., Nechaev, O.Yu., Miasnikov, A.G., Volkov, A.N., 2008. Results of the radiation monitoring system onboard the service module of ISS. In: 13th Workshop on Radiation Monitoring for the International Space Station (WRMISS). Krakow, Poland, September 8–10. Available online at: <http://wrmiss.org/workshops/thirteenth/Benghin.pdf>.
- Benton, E.R., Benton, E.V., 2001. Space radiation dosimetry in low-Earth orbit and beyond. Nucl. Instrum. Methods Phys. Res. B 184 (1–2), 255–294.
- Benton, E., 2005a. Deep space ICCHIBAN: an international comparison of space radiation dosimeters aboard the NASA deep space test bed. In: 10th Workshop for Radiation Monitoring on ISS. Chiba, Japan, 7–9 September. Available online at: http://wrmiss.org/workshops/tenth/pdf/08_benton.pdf.
- Benton, E.R., 2005b. Test of the DSTB passive dosimeter system. ERI Report No. 050901 on the DSTB Certification Flight, prepared for the NASA Space Radiation Shielding Program, Marshall Space Flight Center, work performed under NASA Contract Number NNM05AC80P and NASA Grant Number NNM04AA75G21. September 2005.
- Benton, E.R., Benton, E.V., Frank, A.L., Moyers, M.F., 2006. Characterization of the radiation shielding properties of US and Russian EVA suits using passive detectors. Radiat. Meas. 41, 1191–1201.
- Berger, M.J., Coursey, J.S., Zucker, M.A., Chang, J., 2014. Stopping-power and range tables for electrons, protons, and helium ions. NIST Standard Reference Database 124. Available online at: <http://physics.nist.gov/PhysRefData/Star/Text/contents.html>.
- Burmeister, S., Beaujean, R., Petersen, F., Reitz, G., 2003. Post flight calibration of DOSTEL with heavy ions during the first and third, ICCHIBAN, run at HI-MAC, Chiba. In: 8th Workshop on Radiation Monitoring for the International Space Station 3–5 September 2003. LBNL, Berkeley, USA. Available online at: <http://wrmiss.org/workshops/eighth/burmeister.pdf>.
- Chernykh, I., Petrov, V., Shurshakov, V., et al., 2008. ISS attitude influence on the dose rate measured with Liulin-5 instrument. In: Workshop on Radiation Measurements on ISS. Krakow, Poland, 8–10 September 2008. Available online at: <http://www.wrmiss.org/workshops/thirteenth/Chernykh.pdf>.

- Caffrey, J.A., Hamby, D.M., 2010. A review of instruments and methods for dosimetry in space. *Adv. Space Res.* 47, 563–574. <http://dx.doi.org/10.1016/j.asr.2010.10.005>.
- Dachev, Ts.P., Matviichuk, Yu.N., Semkova, J.V., Koleva, R.T., Boichev, B., Baynov, P., Kanchev, N.A., Lakov, P., Ivanov, Ya.I., Tomov, B.T., Petrov, V.M., Redko, V.I., Kojarinov, V.I., Tykva, R., 1989. Space radiation dosimetry with active detections for the scientific program of the second Bulgarian cosmonaut on board the Mir space station. *Adv. Space Res.* 9 (10), 247–251. [http://dx.doi.org/10.1016/0273-1177\(89\)90445-6](http://dx.doi.org/10.1016/0273-1177(89)90445-6).
- Dachev, Ts., Semkova, J., Petrov, V., Redko, V., Bengin, V., Kostereva, T., Miller, J., Heilbronn, L., Zeitlin, C., 1998a. Analysis of the pre-flight and post-flight calibration procedures performed on the LIULIN space radiation dosimeter. *Acta Astronaut.* 42, 375–387. [http://dx.doi.org/10.1016/S0094-5765\(98\)00132-5](http://dx.doi.org/10.1016/S0094-5765(98)00132-5).
- Dachev, Ts.P., Semkova, J.V., Matviichuk, Yu.N., Tomov, B.T., Koleva, R.T., Baynov, P.T., Petrov, V.M., Shurshakov, V.V., Ivanov, Yu., 1998b. Inner magnetosphere variations after solar proton events. Observations on Mir space station in 1989–1994 time period. *Adv. Space Res.* 22 (4), 521–526. [http://dx.doi.org/10.1016/S0273-1177\(98\)01073-4](http://dx.doi.org/10.1016/S0273-1177(98)01073-4).
- Dachev, Ts.P., Tomov, B.T., Matviichuk, Yu.N., Koleva, R.T., Semkova, J.V., Petrov, V.M., Bengin, V.V., Ivanov, Yu.V., Shurshakov, V.A., Lemaire, J., 1999a. Solar cycle variations of MIR radiation environment as observed by the LIULIN dosimeter. *Radiat. Meas.* 30, 269–274. [http://dx.doi.org/10.1016/S1350-4487\(99\)00061-X](http://dx.doi.org/10.1016/S1350-4487(99)00061-X).
- Dachev, Ts., Tomov, B., Matviichuk, Yu., Dimitrov, Pl., Koleva, R., Semkova, J., Lemaire, J., Petrov, V., Shurshakov, V., 1999b. Overview on the MIR radiation environment results obtained by LIULIN instrument in 1988–1994 time period. Description of LIULIN-4 subsystem for the Russian segment of the ISS. In: *Risk Evaluation of Cosmic-ray Exposure in Long-term Manned Space Mission*. Tokyo, Japan, pp. 127–150.
- Dachev, Ts., Tomov, B., Matviichuk, Yu., Dimitrov, Pl., Lemaire, J., Gregoire, Gh., Cynamukungu, M., Schmitz, H., Fujitaka, K., Uchihori, Y., Kitamura, H., Reitz, G., Beaujean, R., Petrov, V., Shurshakov, V., Bengin, V., Spurny, F., 2002. Calibration results obtained with Liulin-4 type dosimeters. *Adv. Space Res.* 30 (4), 917–925. [http://dx.doi.org/10.1016/S0273-1177\(02\)00411-8](http://dx.doi.org/10.1016/S0273-1177(02)00411-8).
- Dachev, Ts.P., Stassinopoulos, E.G., Tomov, B.T., Dimitrov, Pl.G., Matviichuk, Yu.N., Shurshakov, V.A., Petrov, V.M., 2003. Analysis of the cyclotron facility calibration and aircraft results obtained by LIULIN-3M instrument. *Adv. Space Res.* 32, 67–71. [http://dx.doi.org/10.1016/S0273-1177\(03\)90372-3](http://dx.doi.org/10.1016/S0273-1177(03)90372-3).
- Dachev, T., Atwell, W., Semones, E., Tomov, B., Reddell, B., 2006. ISS Observations of SAA radiation distribution by Liulin-E094 instrument on ISS. *Adv. Space Res.* 37, 1672–1677. <http://dx.doi.org/10.1016/j.asr.2006.01.001>.
- Dachev, Ts.P., 2009. Characterization of near Earth radiation environment by Liulin type instruments. *Adv. Space Res.* 44, 1441–1449. <http://dx.doi.org/10.1016/j.asr.2009.08.007>.
- Dachev, Ts.P., Tomov, B.T., Matviichuk, Yu.N., Dimitrov, P.G., Bankov, N.G., 2009. Relativistic electrons high doses at International space station and Foton M2/M3 satellites. *Adv. Space Res.* 44, 1433–1440. <http://dx.doi.org/10.1016/j.asr.2009.09.023>.
- Dachev, Ts.P., Tomov, B.T., Matviichuk, Yu.N., Dimitrov, Pl.G., Spurny, F., Ploc, O., Brabkova, K., Jadrníková, I., 2011a. Liulin type spectrometry-dosimetry instruments. *Radiat. Prot. Dosim.* 144 (1–4), 675–679. <http://dx.doi.org/10.1093/rpd/ncq506>.
- Dachev, Ts.P., Spurny, F., Ploc, O., 2011b. Characterization of radiation environment by Liulin type spectrometers. *Radiat. Prot. Dosim.* 144 (1–4), 680–683. <http://dx.doi.org/10.1093/rpd/ncq534>.
- Dachev, Ts.P., Tomov, B.T., Matviichuk, Yu.N., Dimitrov, Pl.G., Vadawale, S.V., Goswami, J.N., Girish, V., De Angelis, G., 2011c. An overview of RADOM results for Earth and Moon radiation environment on Chandrayaan-1 satellite. *Adv. Space Res.* 48 (5), 779–791. <http://dx.doi.org/10.1016/j.asr.2011.05.009>.
- Dachev, T.P., Semkova, J., Tomov, B., Matviichuk, Yu., Dimitrov, Pl., Koleva, R., Malchev, St., Reitz, G., Horneck, G., De Angelis, G., Häder, D.-P., Petrov, V., Shurshakov, V., Bengin, V., Chernykh, I., Drobyshev, S., Bankov, N.G., 2011d. Space Shuttle drops down the SAA doses on ISS. *Adv. Space Res.* 47, 2030–2038. <http://dx.doi.org/10.1016/j.asr.2011.01.034>.
- Dachev, T., Tomov, B., Matviichuk, Y., Dimitrov, P., De Angelis, G., Uchihori, Y., Ploc, O., 2011e. Main specifications of new Liulin type intelligent crew personal dosimeter. In: Proceedings of Sixth Scientific Conference with International Participation SES. Sofia, pp. 76–82. ISSN 13131–3888 http://www.space.bas.bg/SENS/SES2010/1_SpPh/11.pdf.
- Dachev, Ts., Horneck, G., Häder, D.-P., Lebert, M., Richter, P., Schuster, M., Demets, R., 2012a. Time profile of cosmic radiation exposure during the EXPOSE-E mission: the R3D instrument. *J. Astrobiol.* 12 (5), 403–411. <http://eea.spaceflight.esa.int/attachments/spacesations/ID501800a9c26c2.pdf>.
- Dachev, Ts.P., Tomov, B.T., Matviichuk, Yu.N., Dimitrov, Pl.G., Bankov, N.G., Reitz, G., Horneck, G., Häder, D.-P., Lebert, M., Schuster, M., 2012b. Relativistic electron fluxes and dose rate variations during April–May 2010 geomagnetic disturbances in the R3DR data on ISS. *Adv. Space Res.* 50, 282–292. <http://dx.doi.org/10.1016/j.asr.2012.03.028>.
- Dachev, Ts., 2013a. Analysis of the space radiation doses obtained simultaneously at 2 different locations outside ISS. *Adv. Space Res.* 52, 1902–1910. <http://dx.doi.org/10.1016/j.asr.2013.08.011>.
- Dachev, T.P., 2013b. Profile of the ionizing radiation exposure between the Earth surface and free space. *J. Atmos. Sol.-Terr. Phys.* 102, 148–156. <http://dx.doi.org/10.1016/j.jastp.2013.05.015>.
- Dachev, Ts., Semkova, J., Tomov, B., Matviichuk, Yu., Dimitrov, P., Bankov, N., Koleva, R., Zelenyi, L., Mitrofanov, I., Malakhov, A., Mokrousov, M., Tretyakov, V., Petrov, V., Shurshakov, V., Bengin, V., 2013a. Bulgarian participation in future interplanetary missions. In: *Proceedings of Seventh Scientific Conference with International Participation SES*. Sofia, 4–6 December 2012, pp. 55–63. ISSN 1313–3888 <http://www.space.bas.bg/SES2012/Ph-5.pdf>.
- Dachev, Ts.P., Tomov, B.T., Matviichuk, Yu.N., Dimitrov, Pl.G., Bankov, N.G., Reitz, G., Horneck, G., Häder, D.-P., Lebert, M., Schuster, M., 2013b. Relativistic electron fluxes and dose rate variations observed on the international space station. *J. Atmos. Sol.-Terr. Phys.* 99, 150–156. <http://dx.doi.org/10.1016/j.jastp.2012.07.007>.
- Dachev, Ts., Horneck, G., Häder, D.-P., Schuster, M., Lebert, M., 2015a. EXPOSE-R cosmic radiation time profile. *J. Astrobiol.* 14, 17–25. <http://dx.doi.org/10.1017/S147355041400093> and http://journals.cambridge.org/article_S147355041400093.
- Dachev, T.P., Tomov, B.T., Matviichuk, Yu.N., Dimitrov, Pl.G., Bankov, N.G., Shurshakov, V.V., Ivanova, O.A., Häder, D.-P., Schuster, M.T., Reitz, G., Horneck, G., 2015b. “BION-M” No. 1 spacecraft radiation environment as observed by the RD3-B3 radiometer-dosimeter in April–May 2013. *J. Atmos. Sol.-Terr. Phys.* 123, 82–91. <http://dx.doi.org/10.1016/j.jastp.2014.12.011>.
- Damasso, M., Dachev, Ts., Falzetta, G., Giardi, M.T., Rea, G., Zanini, A., 2009. The radiation environment observed by Liulin-Photo and R3D-B3 spectrum-dosimeters inside and outside Foton-M3 spacecraft. *Radiat. Meas.* 44, 263–272. <http://dx.doi.org/10.1016/j.radmeas.2009.03.007>.
- Friedberg, W., Snyder, W., Faulkner, D.N., 1992. US FAA Report DOT/FAA/AM-92-2.
- Getley, I.L., Bennett, L.G.I., Lewis, B.J., Bennett, B., Dyer, C.S., Hands, A.D.P., Duldig, M.L., 2010. Evaluation of new cosmic radiation monitors designed for aircrew exposure assessment. *Space Weather* 8, S01001. <http://dx.doi.org/10.1029/2009SW000492>.
- Green, A.R., Bennett, L.G.I., Lewis, B.J., Kitching, F., McCall, M.J., Desormeaux, M., Butler, A., 2005. An empirical approach to the measurement of the cosmic radiation field at jet aircraft altitudes. *Adv. Space Res.* 36, 1618–1626.
- Grigoriev, A.V., Grigoryan, O.R., Drozdov, A.Y., Malyshev, Y.M., Popov, V.V., Mavrev, E.A., Iudin, D.I., 2010. Thunderstorm neutrons in near space: analyses and numerical simulation. *J. Geophys. Res.* 115, A00E52. <http://dx.doi.org/10.1029/2009JA014870>.
- Häder, D.P., Richter, P., Schuster, M., Dachev, Ts., Tomov, B., Dimitrov, Pl., Matviichuk, Yu., 2009. R3D-B2 – measurement of ionizing and solar radiation in open space in the BIOPAN 5 facility outside the FOTON M2 satellite. *Adv. Space Res.* 43 (8), 1200–1211. <http://dx.doi.org/10.1016/j.asr.2009.01.021>.
- Heffner, J., 1971. *Nuclear Radiation and Safety in Space*. M. Atomizdat, p. 115 (in Russian).
- Heynderickx, D., Lemaire, J., Daly, E.J., 1996. Historical review of the different procedures used to compute the L-parameter. *Radiat. Meas.* 26, 325–331.
- Horneck, G., 1994. HZE particle effects in space. *Acta Astronaut.* 32, 749–755.
- Horneck, G., Win-Williams, D.D., Mancinelli, R.L., Cadet, J., Munakata, N., Ronto, G., Edwards, H.G.M., Hock, B., Waenke, H., Reitz, G., Dachev, T., Häder, D.P., Briollet, C., 1998. Biological experiments on the EXPOSE facility of the International Space Station. In: *Proceedings of the 2nd European Symposium – Utilisation of the International Space Station*. ESTEC, Noordwijk, 16–18 November, SP-433, 459–468.
- Hwang, J., Lee, J., Cho, K.-S., Choi, H.-S., Rho, S., Cho, I.-H., 2010. Space radiation measurement on the polar route onboard the Korean commercial flights. *J. Astron. Space Sci.* 27 (1), 43–54.
- Kim, M.-H.Y., De Angelis, G., Cucinotta, F.A., 2010. Probabilistic assessment of radiation risk for astronauts in space missions. *Acta Astronaut.* 68 (7–8), 747–759.
- Kitching, F., 2004. Use of a Liulin detector for the determination of aircrew radiation exposure. Master's thesis. Royal Military College of Canada, Kingston, Ont., Canada, November 2004.
- Kubančák, J., Ambrožová, I., Ploc, O., Pachnerová Brabcová, K., Štěpán, V., Uchihori, Y., 2014. Measurement of dose equivalent distribution on-board commercial jet aircraft. *Radiat. Prot. Dosim.* 162 (3), 215–219. <http://dx.doi.org/10.1093/rpd/nct331>.
- Lantos, P., 1993. The Sun and its effects on the terrestrial environment. *Radiat. Prot. Dosim.* 48 (1), 27–32.
- Markelov, V.V., Redko, V.I., 1981. High sensitivity dosimeter for space radiation. *Kosmich. Issledov.* XIX (2), 316–321.
- McIlwain, C.E., 1961. Coordinates for mapping the distribution of magnetically trapped particles. *J. Geophys. Res.* 66, 3681–3691.
- Matviichuk, Yu.N., Dachev, Ts.P., Tomov, B.T., Dimitrov, Pl.G., 2008. On-line background radiation monitoring using Internet connection. In: *Proceedings of Fundamental Space Research Conference*, pp. 343–346 (in Russian). Available online at: http://www.stil.bas.bg/FSR/PDF/TOP5Matviichuk_Yuri211249.pdf.
- Mertens, C.J., Meier, M.M., Brown, S., Norman, R.B., Xu, X., 2013. NAIRAS aircraft radiation model development, dose climatology, and initial validation. *Space Weather* 11, 1–33. <http://dx.doi.org/10.1002/swe.20100>.

- Mertens, C.J., Kress, B.T., Wiltberger, M., Tobiska, W.K., Grajewski, B., Xu, X., 2012. Atmospheric ionizing radiation from galactic and solar cosmic rays. In: Nenoi, Mitsuru (Ed.), Current Topics in Ionizing Radiation. InTech Publisher (ISBN 978-953-51-0196-3) <http://www.intechopen.com/articles/show/title/atmospheric-ionizing-radiation-from-galactic-and-solar-cosmic-rays>.
- Mertens, C.J., Kress, B.T., Wiltberger, M., Blattnig, S.R., Slaba, T.S., Solomon, S.C., Engel, M., 2010. Geomagnetic influence on aircraft radiation exposure during a solar energetic particle event in October 2003. *Space Weather* 8, S03006. <http://dx.doi.org/10.1029/2009SW000487>.
- Mitaroff, A., Silari, M., 2002. The CERN-EU high energy reference field (CERF) facility for dosimetry at commercial flight altitudes and in space. *Radiat. Prot. Dosim.* 102, 7–22.
- Nealy, J.E., Cucinotta, F.A., Wilson, J.W., Badavi, F.F., Zapp, N., Dachev, T., Tomov, B.T., Semones, E., Walker, S.A., De Angelis, G., Blattnig, S.R., Atwell, W., 2007. Pre-engineering spaceflight validation of environmental models and the 2005 HZETRN simulation code. *Adv. Space Res.* 40 (11), 1593–1610. <http://dx.doi.org/10.1016/j.asr.2006.12.030>.
- O'Brien, K., Felsberger, E., Kindl, P., 2005. Application of the heliocentric potential to aircraft dosimetry. *Radiat. Prot. Dosim.* 116, 336–342.
- Petrov, V.L., Panasyuk, M.I., Amelyushkin, A.M., Drozdov, A.Yu., Nechaev, O.Yu., 2010. RAZREZ system for RADIOSCAF experiment. In: Fourteenth WRMIS Workshop. Dublin, UK, 7–9 September 2010. Available online at: <http://www.wrmis.org/workshops/fourteenth/Petrov.pdf>.
- Ploc, O., Spurný, F., Dachev, Ts.P., 2011. Use of energy depositing spectrometer for individual monitoring of aircrew. *Radiat. Prot. Dosim.* 144 (1–4), 611–614. <http://dx.doi.org/10.1093/rpd/ncq505>.
- Ploc, O., 2009. Measurement of exposure to cosmic radiation at near-Earth vicinity with energy deposition spectrometer Liulin onboard aircraft and spacecraft. PhD thesis, September 2009.
- Ploc, O., Ambrožová, I., Kubančák, J., Kovář, I., Dachev, Ts., 2013. Publicly available database of measurements with the silicon spectrometer Liulin on board aircraft. *Radiat. Meas.* 58, 107–112. <http://dx.doi.org/10.1016/j.radmeas.2013.09.002>.
- Radiation Protection 140, 2004. Cosmic radiation exposure of aircraft crew, compilation of measured and calculated data. In: Lindborg, L., Bartlett, D.T., Beck, P., McAulay, I.R., Schnuer, K., Schraube, H., Spurný, F. (Eds.), Final Report of EURADOS WG 5, Group of Experts established under Article 31 of the Euratom treaty, Directorate-General for Energy and Transport, Directorate H – Nuclear Energy, Unit H.4 – Radiation Protection. Available online at: http://ec.europa.eu/energy/nuclear/radiation_protection/doc/publication/140.pdf.
- Reitz, G., Beaujean, R., Benton, E., Burmeister, S., Dachev, Ts., Demer, S., Luszik-Bhadra, M., Olko, P., 2005. Space radiation measurements on-board ISS-the DOSMAP experiment. *Radiat. Prot. Dosim.* 116, 374–379. <http://rpd.oxfordjournals.org/cgi/content/abstract/116/1-4/374>.
- Reitz, G., Berger, T., Matthiae, D., 2012. Radiation exposure in the moon environment. *Planet. Space Sci.* 74, 78–83.
- Sáez Vergara, J.C., Dominguez-Mompell, R., 2009. The implementation of cosmic radiation monitoring in routine flight operation of IBERIA airline of Spain: 1 year of experience of in-flight permanent monitoring. *Radiat. Prot. Dosim.* 136, 291–296.
- Schuster, M., Dachev, Ts., Richter, P., Häder, D.-P., Lebert, M., 2012. R3DE, Radiation risk radiometer-dosimeter on the international space station (ISS) – radiation data recorded during 18 month of EXPOSE-E exposure to open space climate. *J. Astrobiol.* 12 (5), 393–402. <http://dx.doi.org/10.1089/ast.2011.0743>.
- Semkova, J., Dachev, Ts., Matviichuk, Yu., Koleva, R., Tomov, B., Bajnov, P., Petrov, V., Nguyen, V., Siegrist, M., Chene, J., d'Uston, C., Cotin, F., 1994. Dosimetric investigation on MARS-96 missions. *Adv. Space Res.* 14 (10), 707–710. [http://dx.doi.org/10.1016/0273-1177\(94\)90530-4](http://dx.doi.org/10.1016/0273-1177(94)90530-4).
- Semkova, J., Koleva, R., Todorova, G., Kanchev, N., Petrov, V., Shurshakov, V., Benghin, V., Tchhernykh, I., Akatov, Yu., Redko, V., Ivanov, Yu., 2003. Investigation of dose and flux dynamics in the Liulin-5 dosimeter of the tissue-equivalent phantom onboard the Russian segment of the International Space Station. *Adv. Space Res.* 31, 1383–1388.
- Semkova, J., Koleva, R., Shurshakov, V., Benghin, V., Maltchev, St., Kanchev, N., Petrov, V., Yarmanova, E., Chernykh, I., 2007. Status and calibration results of Liulin-5 charged particle telescope designed for radiation measurements in a human phantom onboard the ISS. *Adv. Space Res.* 40, 1586–1592. <http://dx.doi.org/10.1016/j.asr.2007.01.008>.
- Semkova, J., Maltchev, S., Tomov, B., Matviichuk, Yu., Dachev, Ts., Koleva, R., Benghin, V., Chernykh, I., Shurshakov, V., Petrov, V., 2008. Charged particle telescope Liulin-Phobos for radiation environment study during upcoming Phobos Sample Return Mission. In: Proceedings of the International Conference on Fundamental Space Research. Sunny Beach, Bulgaria, 23–28 September 2008, pp. 351–354. ISBN 978-954-322-316-9. Available online at: <http://www.stil.bas.bg/FSR2009/>.
- Semkova, J., Maltchev, St., Benghin, V., Uchihori, Y., Yasuda, N., Kitamura, H., 2009. Results of Liulin-F particle telescope pre-flight calibrations with protons and heavy ions. In: Proceedings of Fundamental Space Research Conference, pp. 211–214. <http://www.stil.bas.bg/FSR2009/>.
- Semkova, J., Koleva, R., Maltchev, St., et al., 2010. Radiation measurements inside a human phantom aboard the International Space Station using Liulin-5 charged particle telescope. *Adv. Space Res.* 45 (7), 858–865. <http://dx.doi.org/10.1016/j.asr.2009.08.027>.
- Semkova, J., Koleva, R., Maltchev, St., Bankov, N., Benghin, V., et al., 2012. Depth dose measurements with the Liulin-5 experiment inside the spherical phantom of the Matroska-R project onboard the International Space Station. *Adv. Space Res.* 49, 471–478. <http://dx.doi.org/10.1016/j.asr.2011.10.005>.
- Semkova, J., Koleva, R., Maltchev, St., Bankov, N., Benghin, V., et al., 2013a. Radiation characteristics in the spherical tissue-equivalent phantom on the ISS during solar activity minimum according the data from Liulin-5 experiment. *J. Atmos. Sol-Terr. Phys.* 99, 157–163. <http://dx.doi.org/10.1016/j.jastp.2012.07.006>.
- Semkova, J., Koleva, R., Bankov, N., Malchev, St., Petrov, V.M., et al., 2013b. Study of radiation conditions onboard the International space station by means of the Liulin-5 dosimeter. *Cosm. Res.* 51, 124–132. <http://dx.doi.org/10.1134/S0010952512060068>.
- Semkova, J., Dachev, T., Koleva, R., Maltchev, S., Bankov, N., et al., 2013c. Radiation environment on the international space station during the solar particle events in March 2012. *Astrobiol. Outreach* 1, 102. <http://dx.doi.org/10.4172/jao.1000102>.
- Semones, E., 2008. ISS TEPC measurement results. In: 13th Workshop on Radiation Monitoring for the International Space Station (WRMISS). Krakow, Poland, September 8–10, 2008. Available online at: http://wrmiss.org/workshops/thirteenth/Semones_TEPC.pdf.
- Shea, M.A., Smart, D.F., 2001. Vertical cutoff rigidities for cosmic ray stations since 1955. In: 27th International Cosmic Ray Conference. Contributed Papers, vol. 10, pp. 4063–4066.
- Shurshakov, V.A., Petrov, V.M., Ivanov, Yu.V., Bondarenko, V.A., Tzetlin, V.V., Makhmutov, V.S., Dachev, Ts.P., Semkova, J.V., 1999. Solar particle events observed on MIR station. *Radiat. Meas.* 30, 317–325. [http://dx.doi.org/10.1016/S1350-4487\(99\)00058-X](http://dx.doi.org/10.1016/S1350-4487(99)00058-X).
- Shurshakov, V., Akatov, Y., Kartsev, I.S., et al., 2006. Measurements of the absorbed dose distribution in the spherical tissue equivalent phantom in MATROSHKA-R space experiment. In: 11th WRMISS. United Kingdom, Oxford. Available online at: <http://www.wrmis.org/workshops/eleventh>, 2006.
- Simpson, J.A., 1983. Composition and origin of cosmic rays. In: Shapiro, M.M. (Ed.), *NATO Adv. Stud. Inst. Ser. Ser. C Math. Phys. Sci.*, vol. 107. Reidel, Dordrecht.
- Slaba, T.C., Blattnig, S.R., Badavi, F.F., Stoffle, N.N., Rutledge, R.D., Lee, K.T., Zapp, E.N., Dachev, T.P., Tomov, B.T., 2011. Statistical validation of HZETRN as a function of vertical cutoff rigidity using ISS measurements. *Adv. Space Res.* 47, 600–610. <http://dx.doi.org/10.1016/j.asr.2010.10.021>.
- Spurný, F., 2000. Dosimetry measurements during a balloon flight – June 2000. Report DRD NPI AS CR 488/00.
- Spurný, F., 2005. Response of a Si-diode-based device to fast neutrons. *Radiat. Meas.* 39, 219–223. <http://dx.doi.org/10.1016/j.radmeas.2004.05.006>.
- Spurný, F., Dachev, Ts., 2003. Long-term monitoring of the onboard aircraft exposure level with a Si-diode based spectrometer. *Adv. Space Res.* 32 (1), 53–58. [http://dx.doi.org/10.1016/S0273-1177\(03\)90370-X](http://dx.doi.org/10.1016/S0273-1177(03)90370-X).
- Spurný, F., Ploc, O., Jadrníková, I., 2009. Spectrometry of linear energy transfer and dosimetry measurements onboard spacecrafts and aircrafts. *Phys. Part. Nucl. Lett.* 6, 70–77. # Pleiades Publishing, Ltd. ISSN 2009, 1547–4771.
- Stassinopoulos, E.G., Stauffer, C.A., Dachev, T.P., Brucker, C.J., Tomov, B.T., Dimitrov, P.G., 2002. The LIULIN-3M radiometer for measuring particle doses in space and on aircraft. NASA/TM-2002-210003, February 2002, Available online at: http://ntrs.nasa.gov/archive/nasa/casi.ntrs.nasa.gov/20020045343_2002075693.pdf.
- Streb, C., Richter, P., Lebert, M., Dachev, T., Häder, D.-P., 2002. R3D-B, radiation risk radiometer-dosimeter on biopan (Foton) and EXPOSE on International space station. In: *Proceedings of the Second Exo-Astrobiology Workshop*. Graz, Austria. In: ESA, vol. SP-518. ISBN 92-9092-828-X, pp. 71–74.
- Tomov, B., Dimitrov, Pl., Matviichuk, Yu., Dachev, Ts., 2008. Galactic and solar cosmic rays study by ground and rocketborne space radiation spectrometers-dosimeters – Liulin-6R and Liulin-R. In: *Proceedings of Fundamental Space Research Conference*, pp. 252–257. ISBN 978-954-322-316-9, Available online at: http://www.stil.bas.bg/FSR/PDF/TOP5Tomov_Borislav2242058.pdf.
- Uchihori, Y., Kitamura, H., Fujitaka, K., Dachev, Ts.P., Tomov, B.T., Dimitrov, P.G., Matviichuk, Yu., 2002. Analysis of the calibration results obtained with Liulin-4J spectrometer-dosimeter on protons and heavy ions. *Radiat. Meas.* 35, 127–134.
- Uchihori, Y., Dachev, T., Kitamura, H., Kentaro, H., Yajima, K., 2003a. Chapter VII – Liulin-4J silicon portable spectrometer. Report, HIMAC-078, pp. 56–63.
- Uchihori, Y., Kitamura, H., Fujitaka, K., Yasuda, N., Benton, E., 2003b. Comparison of results from the 1st ICCHIBAN experiment and current status of the 3rd ICCHIBAN experiment. In: 8th Workshop on Radiation Monitoring for the International Space Station. 3–5 September, LBNL, Berkeley, USA, 2003. Available online at: <http://wrmiss.org/workshops/eighth/uchihori.pdf>.
- Uchihori, Y., Benton, E., Moeller, J., Bendrick, G., 2003c. Radiation measurements aboard NASA ER-2 high altitude aircraft with the Liulin-4J portable spectrometer. *Adv. Space Res.* 32, 41–46.
- Uchihori, Y., Benton, E.R., Yasuda, N., et al., 2005. ICCHIBAN Working Group and ICCHIBAN participants NSRL-ICCHIBAN Brief Report, ICCHIBAN-7&8 Announcement and Future ICCHIBAN experiments. In: 10th WRMISS. Chiba, Japan, 2005. Available online at: http://wrmiss.org/workshops/tenth/pdf/01_uchihori.pdf.

- Wahl, L.E., 2010. Environmental radiation. Available online at: http://hps.org/documents/environmental_radiation_fact_sheet.pdf. Fig. 1, reprinted from <http://www.ncrppublications.org/Reports/160>.
- Wilson, J.W., Maiden, D.L., Goldhagen, P., Tai, H., Shinn, J.L., 2003. Overview of Atmospheric Ionizing Radiation (AIR), NASA Langley research Center, 2003. Available online at: http://ntrs.nasa.gov/archive/nasa/casi.ntrs.nasa.gov/20030063010_2003072785.pdf.
- Wilson, J.W., Nealy, J.E., Dachev, T., Tomov, B.T., Cucinotta, F.A., Badavi, F.F., De Angelis, G., Leutke, N., Atwell, W., 2007. Time serial analysis of the induced LEO environment within the ISS 6A. *Adv. Space Res.* 40 (11), 1562–1570. <http://dx.doi.org/10.1016/j.asr.2006.12.030>.
- Wissmann, F., Burda, O., Khurana, S., Klages, T., Langner, F., 2013. Dosimetry of secondary cosmic radiation up to an altitude of 30 km. *Radiat. Prot. Dosim.* 161 (1–4), 299–302. <http://dx.doi.org/10.1093/rpd/nct329>.
- Zapp, N., 2013. NASA GSFC, by 'Coordinated Data Analysis Web' at Goddard Space Flight Center. <http://cdaweb.gsfc.nasa.gov/tmp/>.
- Zhang, L., Mao, R., Zhu, R., 2011. Fast neutron induced nuclear counter effect in Hamamatsu silicon PIN diodes and APDs. *IEEE Trans. Nucl. Sci.* 58 (3), 1249–1256.
- Zheng, Y., Lui, A.T.Y., Li, X., Fok, M.C., 2006. Characteristics of 2–6 MeV electrons in the slot region and inner radiation belt. *J. Geophys. Res.* 111, 2006. A10204.